## TITU MAIORESCU UNIVERSITY OF BUCHAREST IOSUD

Field of Study: MEDICINE

# DOCTORAL DISSERTATION

# STUDY OF THE SYNERGISM BETWEEN HEPATIC PHYTOTHERAPY AND HEPATIC ONCOTHERAPY ABSTRACT

**Scientific Supervisor** 

Professor Dr. DAN FLORIN UNGUREANU

PhD Candidate Mirela Claudia RÎMBU

BUCHAREST

2025

#### TABLE OF CONTENTS

CHAPT	ER VI	ANT	OXIDA	NT AND	ANTIE	BACTE	RIAL	ACTIV	TTY OF	EXT	CRACTS
FROM	<b>CLEM</b>	ATIS H	HERBA,	<b>MELISS</b>	AE FOL	IUM,	TARAX	ACI H	ERBA,	AND	SILYBII
FRUCT	US										

6.1 Quantitative Determination of Polyphenolic Compounds	86
6.2 Antioxidant Activity	
6.3 Antimicrobial Activity	89
6.4 Conclusions	92
CHAPTER VII: IN VITRO SYNERGISM BETWEEN GREEN-SYNTH	
NANOPARTICLES AND LATEST-GENERATION ANTITUMORAL DRUGS O LINES	N CELL
	02
7.1 Introduction	
7.3 <i>In Vitro</i> Antitumor Testing	
7.4 Conclusions	
CHAPTER VIII: MOLECULAR DOCKING STUDY OF ACTIVE PRINCIPLES MEDICINAL PLANTS AND TYROSINE KINASE INHIBITORS	S FROM
8.1 Preparation and Characterization of Receptor Structures	119
8.2 Preparation and Characterizatin of Ligant Structures	
8.3 Molecular Docking	142
CHAPTER IX: EVALUATION OF ADVERSE EFFECTS AND SAFE ONCOTHERAPIES	TY OF
9.1 Introduction	153
9.2 Pharmacovigilance of Cisplatin	
9.3 Pharmacovigilance of Tyrosine Kinase Inhibitors	
9.4 Conclusions	175
CHAPTER X: CASE STUDY: PHGIST – GIANT INTRAHEPATIC STROMAL	ГUMOR
10.1 Introduction	176
10.2 Clinical Case Stages	
10.3 Clinical Particularities of the Case	
10.4 Comparative Analysis of Biochemical Data	
10.5 Biochemical Particularities of the Case	
10.6 Conclusions	228
GENERAL CONCLUSIONS	229
BIBLIOGRAPHY	232
Annex 1 – Figures Index	
Annex 2 – Tables Index	
Annex 3 – Ethics Approvals	
Annex 4 – Index of Scientific Works	

#### **INTRODUCTION**

In recent years, research in the field of oncology has focused on developing more effective and better-tolerated therapies for the treatment of solid tumors. Gastrointestinal stromal tumors (GISTs) represent a relevant example of neoplasms with complex biological behavior, characterized by an initial sensitivity to targeted therapies, often followed by the development of secondary resistance. Although current treatments, such as tyrosine kinase inhibitors (TKIs), have significantly improved the prognosis of patients with GIST - especially those who are inoperable or have metastatic disease - long-term survival remains variable, and treatment resistance poses a major challenge.

This research was initiated based on the analysis of a particular clinical case involving a 71-year-old female patient at the time of diagnosis, in March 2017, with a rare form of giant GIST originating in the liver (PHGIST). The patient underwent surgery at the time of diagnosis and was started on Imatinib, a first-line TKI. The evolution was favorable for five years; however, in 2022, resistance to treatment was observed, necessitating a second surgical intervention and the switch to Sunitinib, used as second-line therapy. The patient's overall survival was 8 years, of which five were under Imatinib and two under Sunitinib, until February 2025. This case raises essential questions regarding the mechanisms of resistance to current treatments and the possibility of improving therapeutic strategies by adding adjuvant agents to delay or prevent resistance development.

In this context, the present study explores the potential use of biosynthesized silver nanoparticles and plant extracts in oncological therapy, focusing on their impact on cell viability and their potential synergism with conventional chemotherapeutic drugs. Metallic nanoparticles - especially silver ones - have shown significant cytotoxic activity against tumor cells, while being less toxic to healthy cells compared to standard chemotherapeutics. At the same time, plant extracts, rich in bioactive compounds such as polyphenols and alkaloids, have shown promising potential in inhibiting cell proliferation and inducing apoptosis, making them candidates for use as adjuvants in cancer therapies. In vitro test results demonstrated that dandelion-extract-derived biosynthesized nanoparticles exert a dose- and time-dependent cytotoxic effect on tumor cells, showing intermediate activity between Cisplatin - a standard chemotherapeutic agent - and simple plant extracts. Additionally, greater celandine (*Chelidonium majus*) extract demonstrated antitumor activity superior to Cisplatin on HepG2 cells, especially after 48 hours of treatment. These findings support the hypothesis that plant secondary metabolites may enhance the efficacy

of conventional treatments either through direct cytotoxic effects or via synergistic action with chemotherapeutic agents.

Another important aspect of this research is the investigation of interactions between tyrosine kinase inhibitors and biosynthesized nanoparticles. The combined administration of Sunitinib and Imatinib with silver nanoparticles resulted in increased antitumor efficacy, reducing tumor cell viability while protecting normal HUVEC cells. These results suggest that combined therapies could represent a promising strategy to enhance treatment response and prolong the effectiveness of tyrosine kinase inhibitors, thereby delaying resistance development.

In addition to cytotoxicity studies, this research also examined the antioxidant and antimicrobial properties of plant extracts. Species such as *Melissa officinalis* and *Clematis vitalba* demonstrated strong antioxidant activity due to their high polyphenol content, suggesting a possible protective role against oxidative stress - a factor involved in cancer progression. Furthermore, microbiological testing indicated significant antibacterial activity, opening new directions for the use of these extracts in infection prevention and treatment, particularly in oncologic patients with compromised immunity. Complementing the experimental analyses, molecular docking techniques were employed to identify novel molecules with therapeutic potential. The results highlighted the presence of ligands with high affinities for receptors involved in cell proliferation, suggesting the possibility of using these compounds in the development of more effective and better-tolerated chemotherapeutic agents.

Finally, the pharmacovigilance analysis of the drugs used in oncological therapy revealed that both Imatinib and Sunitinib are associated with frequent and severe adverse reactions, especially in elderly patients. The toxicity profile of these medications necessitates rigorous monitoring and dose optimization tailored to each patient's individual response to treatment.

This dissertation aims to evaluate the efficacy and safety of biosynthesized nanoparticles and plant extracts as potential therapeutic or adjuvant agents in cancer treatment, using as a starting point the case of a patient with PHGIST who survived eight years under conventional therapies. Through an interdisciplinary approach, the thesis will examine the impact of these agents on cell viability, their mechanisms of action, interactions with standard therapies, and the pharmacological implications of their use. The ultimate goal of the research is to contribute to the development of therapeutic strategies that improve the effectiveness of oncological treatments and reduce their toxicity, thereby offering patients safer and better-tolerated options.

### CHAPTER III: STAGING OF PATIENTS WITH HEPATIC ONCOLOGICAL PATHOLOGY

#### 3.1 Introduction

The classification of cancer cases based on the anatomical extent of the disease, known as staging, originated from the observation that patients with localized tumors had higher survival rates than those in whom the disease had spread beyond the initial organ. The stage identified at diagnosis reflects not only the speed of tumor growth and dissemination but also its type and the interaction between cancer cells and the host organism.

Accurate recording of the anatomical extent of the disease at the time of diagnosis is essential for: treatment planning by the physician, estimation of patient prognosis, assessment of treatment efficacy, facilitating information exchange between medical centers, ongoing cancer research, and supporting cancer control strategies.

Staging plays a central role in patient care, research, and disease control measures. These measures include individualized care, development of clinical guidelines, and data recording for population-level disease monitoring. Accurate stage classification helps evaluate treatment outcomes and the effectiveness of oncology programs. However, to assess the long-term impact of the disease, the classification system must remain stable, which poses a challenge between updating it according to the latest medical findings and maintaining continuity for longitudinal studies.

#### 3.2. Materials and Methods

The present study included 568 patients with suspected hepatic tumors, hospitalized in two medical centers in Bucharest: Fundeni Clinical Institute and Bucharest Emergency Clinical Hospital. Staging was performed according to the TNM system, using both clinical classification (cTNM) and pathological classification (pTNM), depending on the availability of postoperative data.

The studied parameters included: patient age and sex, classification of hepatic tumors according to UICC criteria (T, N, M), distribution by stage (I–IV, including substages a/b), tumor location and lymph node invasion, as well as the presence or absence of metastases.

The data were retrospectively collected from medical records based on the ethics approvals issued by the Clinical Institute Fundeni (no. 5270/30.09.2024) and the Emergency Clinical Hospital (no. 7209/11.09.2024). The data was centralized and statistically analyzed using Microsoft Office (Excel, 2024) and IBM SPSS Statistics software.

#### 3.3. Results and Discussion

#### 3.3.1. Demographic Characteristics

Among the 568 patients, 51.6% were male and 48.4% were female, with the majority falling within the 65–85 age group (57.38%).

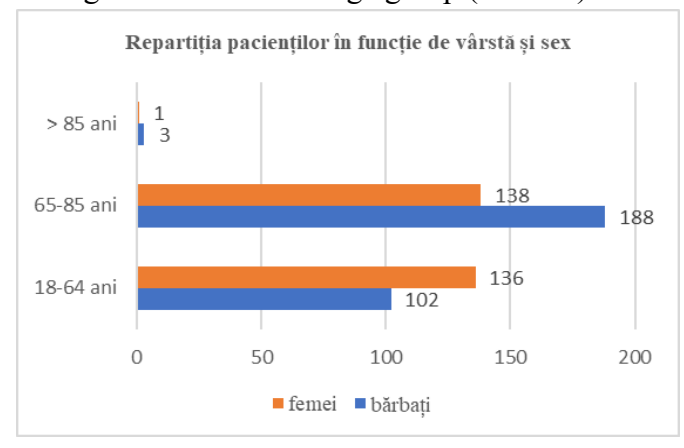


Figure 3.1: Distribution of patients by age and sex

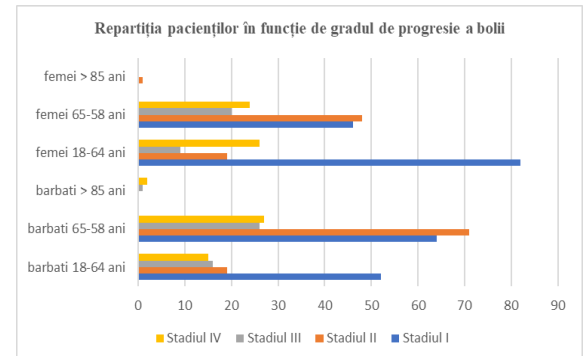
Testing the proportion equality between the number of female and male patients yielded the following results

$$Z = 0.763 \in (-1.65; 1.65),$$
 and

p = 0.4454 > 0.10, indicating no statistically significant difference between sexes.

#### 3.3.2. Stage Distribution

According to disease severity, 43% of patients were in stage I, 27.8% in stage II, 12.7% in stage III, and 16.5% in stage IV.



The statistical test is:

$$\chi^2_{(2-1)(4-1)} = \chi^2_3 = \sum_{i=1}^{10} \frac{(o_i - E_i)^2}{E_i} = \frac{(116 - 125, 9)^2}{125, 9} + \dots + \frac{(50 - 45, 5)^2}{45, 5} = 6,19$$

with a critical value of 7,815.

Thus, the distribution of disease stages did not depend on the patient's sex.

Figure 3.2: Patient distribution according to disease progression

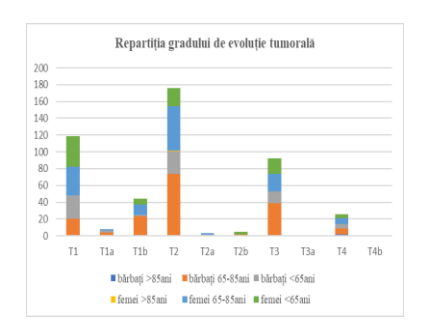
When analyzing patient distribution across substages a, b, and c, it was observed that no patients were classified as substage c. A total of 97.54% of patients were in substage a, while 2.46% were in substage b. Notably, 98% of female patients and 97% of male patients were in substage a.

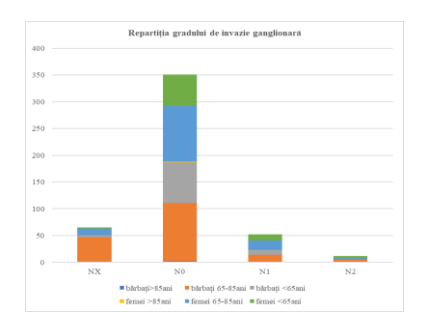
Tabel III.2: Substage a, b, c

Sex	Age	Substage a	Substage b	Substage c	In the 65–85 age group, 61.77% of men and
Men	>85 y	3	0	0	49.82% of women were in substage a, a
	65-85 y	181	7	0	statistically significant difference (Z =
	<65 y	101	1	0	4.357).
Women	>85 y	1	0	0	In the group under 65 years, the distribution
	65-85 y	137	1	0	differed: 34.47% of men versus 47.64% of
	<65 y	131	5	0	women ( $Z = 4.115$ ), also statistically
					significant.

#### 3.3.3. TNM Parameters

Tumors (T) Regional Nodes (N) Metastases (M)





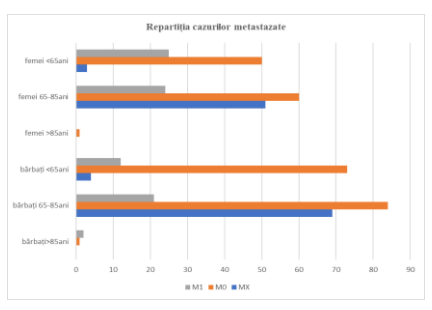


Figure 3.6: Distribution by tumor progression grade

Figure 3.7: Distribution by lymph node invasion grade

Figure 3.8: Distribution of metastatic cases

The most frequent tumor stages were T2 (37.05%), T1 (25.05%), and T3 (19.37%), while the least common were T3a and T4b, each at 0.21%. Regarding lymph node invasion, 73.13% of cases had no nodal involvement (N0), 10.83% were N1, 2.50% were N2, and 13.54% had multiple invasions. Most cases occurred in the 65–85 age group (36.25% of men and 28.54% of women). For metastasis status, 26.46% were classified as MX, 56.04% as M0, and 17.50% as M1.

#### 3.4. Conclusions

The data collected indicates a high prevalence of early-stage tumors (stages I and II), with 70.8% of patients classified in these categories. T2-type tumors were the most frequently encountered (37.05%), especially among patients aged 65–85, supporting international data that report a higher incidence of hepatic cancer in the elderly and its association with pre-existing chronic conditions (cirrhosis, viral hepatitis, metabolic syndromes).

Regarding lymph node invasion, a significant proportion of patients (73.13%) showed no lymphatic involvement (N0), and multiple invasions (N2) were rare (2.5%), suggesting a predominantly locoregional evolution in early stages.

Additionally, in the substage analysis (a, b, c), the vast majority of cases fell into substage a, with no statistically significant sex-related differences.

Distant metastases (M1) were identified in 17.5% of cases, while 26.46% of patients had an unknown metastatic status (MX), highlighting the need for improved imaging and pathological documentation.

In conclusion, this study emphasizes the importance of rigorously applying international staging systems, adapted to the local characteristics of hepatic oncological pathology, and underlines the ongoing need to improve early diagnostic tools, complementary investigations, and individualized therapeutic strategies based on the patient's TNM profile.

# CHAPTER V: SYNTHESIS AND CHARACTERIZATION OF SILVER NANOPARTICLES BASED ON *TARAXACI HERBA* EXTRACT AND EVALUATION OF CYTOTOXIC ACTIVITY ON HEPG2 CELL LINE

#### 4.1 Introduction

Dandelion (*Taraxacum officinale*) is a valuable medicinal plant due to its high content of bioactive compounds such as sesquiterpenes, flavonoids, sterols, and polysaccharides. These compounds endow the plant with remarkable pharmacological properties, including anti-inflammatory, antioxidant, antibacterial, and antitumor activities.

In this study, gold nanoparticles (AuNPs) and silver nanoparticles (AgNPs) were synthesized using ethanolic and aqueous dandelion extracts through a green synthesis method. The nanoparticles were characterized by UV-Vis spectroscopy, scanning electron microscopy (SEM), dynamic light scattering (DLS), and electrophoretic light scattering (ELS). The cytotoxic activity of these nanoparticles was evaluated on HepG2 cells using the MTS cell viability assay. Results indicated a significant antitumor effect of the alcoholic dandelion extract, especially after 48 hours of exposure, comparable to or even exceeding the effect of Cisplatin (CisPt).

The aim of this study is to synthesize and characterize AgNPs derived from dandelion extract and to assess their cytotoxic activity on HepG2 cancer cells.

#### 4.2 Materials and Methods

#### Nanoparticle synthesis

The following samples were used for nanoparticle synthesis:

- AgNPsEaq-D Colloidal silver obtained from aqueous dandelion extract
- AgNPsEETOH5%D Colloidal silver obtained from 50% ethanolic extract
- EETOH-D Ethanolic extract of dandelion
- Eaq-D Aqueous extract of dandelion

#### Nanoparticle characterization

- UV-Vis spectroscopy was performed using a U-0080D UV-Vis spectrophotometer (Hitachi, Japan)
- SEM analysis was conducted using the Nova NanoSEM 630 (FEI Company, USA)
- DLS and ELS were used to determine particle size and Zeta potential (Delsa Nano C, Beckman Coulter, USA)

#### MTS Toxicity Test

The MTS assay was used to evaluate the cytotoxic effect of the nanoparticles on HepG2 cells. A total of  $1 \times 10^4$  cells/well were incubated for 24 hours, followed by exposure to extracts and oncolytic drugs for 24 and 48 hours. Then, 20  $\mu$ L of MTS reagent was added, and plates were incubated at 37°C for 4 hours. Absorbance was read at 492 nm, and cell viability was calculated relative to the untreated control (considered 100%).

#### 4.3 Results and Discussion

#### Physicochemical characterization of nanoparticles

UV-Vis spectroscopy confirmed the reduction of silver nitrate by dandelion extract, with an absorption band at 457 nm for aqueous extract-based AgNPs and 450 nm for ethanolic extract-based AgNPs (Figure 4.1).

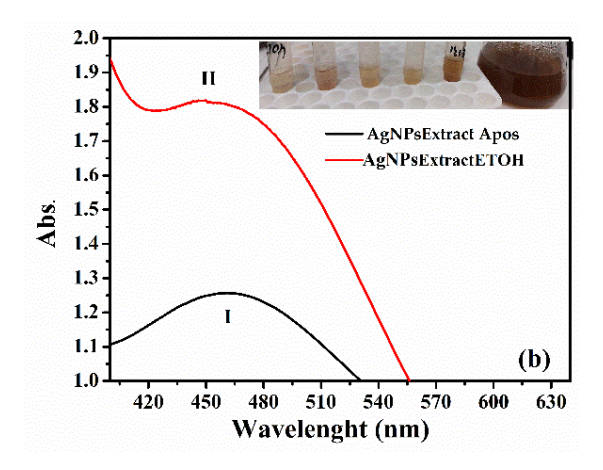


Figure 4.1: UV-Vis spectra for AgNPs synthesized from aqueous (I) and ethanolic (II) dandelion extracts

The size distribution of AuNPsEETOH-D was obtained from the SEM image (Figure 4.2) by measuring approximately 400 nanoparticles. ImageJ software was used to extract the necessary data from the SEM micrographs and to compile the histograms. It was found that the nanoparticle sizes ranged from 11 nm to 43 nm for the AuNPsEETOH-D sample.

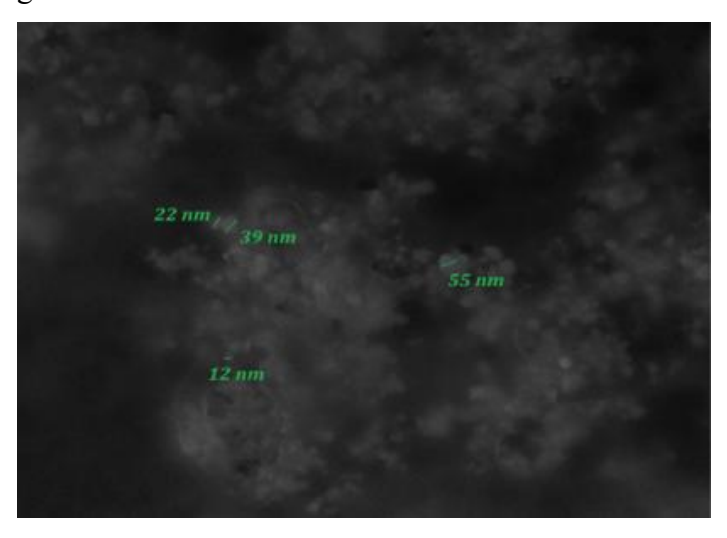


Figure 4.2: SEM image of AgNPs;

These data were then compiled into histograms, which were best fitted with a Gaussian function to accurately represent the distribution. The highest percentage of nanoparticles in the AuNPsEETOH-D sample was found in the 16–24 nm range, as shown in Figure 4.3.

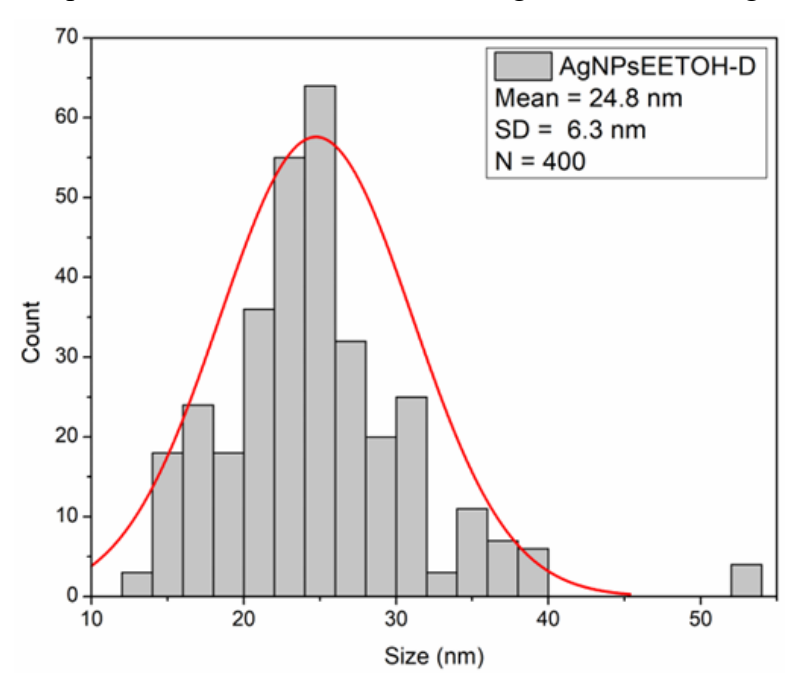


Figure 4.3: Size distribution histogram for AuNPsEETOH-D

DLS analysis showed that AgNPsEaqD had a smaller hydrodynamic diameter (337.4 nm) than AgNPsEETOH-D (500 nm) – Figure 4.4 vs Figure 4.5.

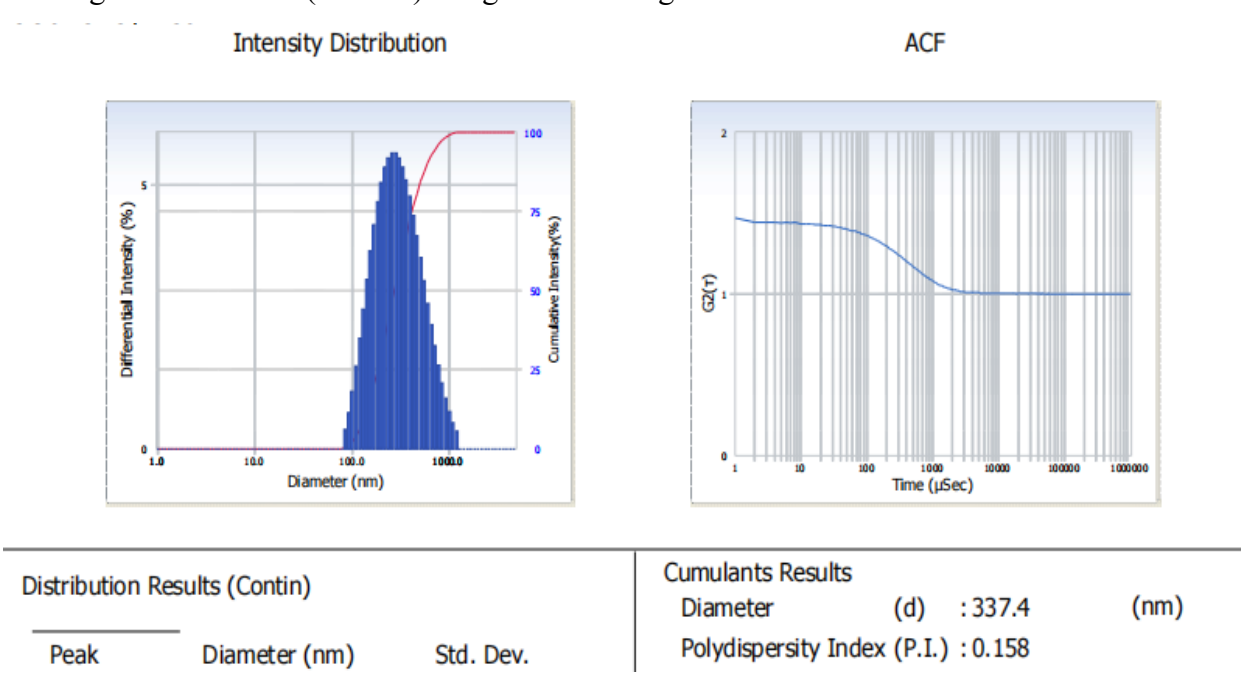


Figure 4.4: Hydrodinamic diameter, polydispersity index for AgNPsEaqD

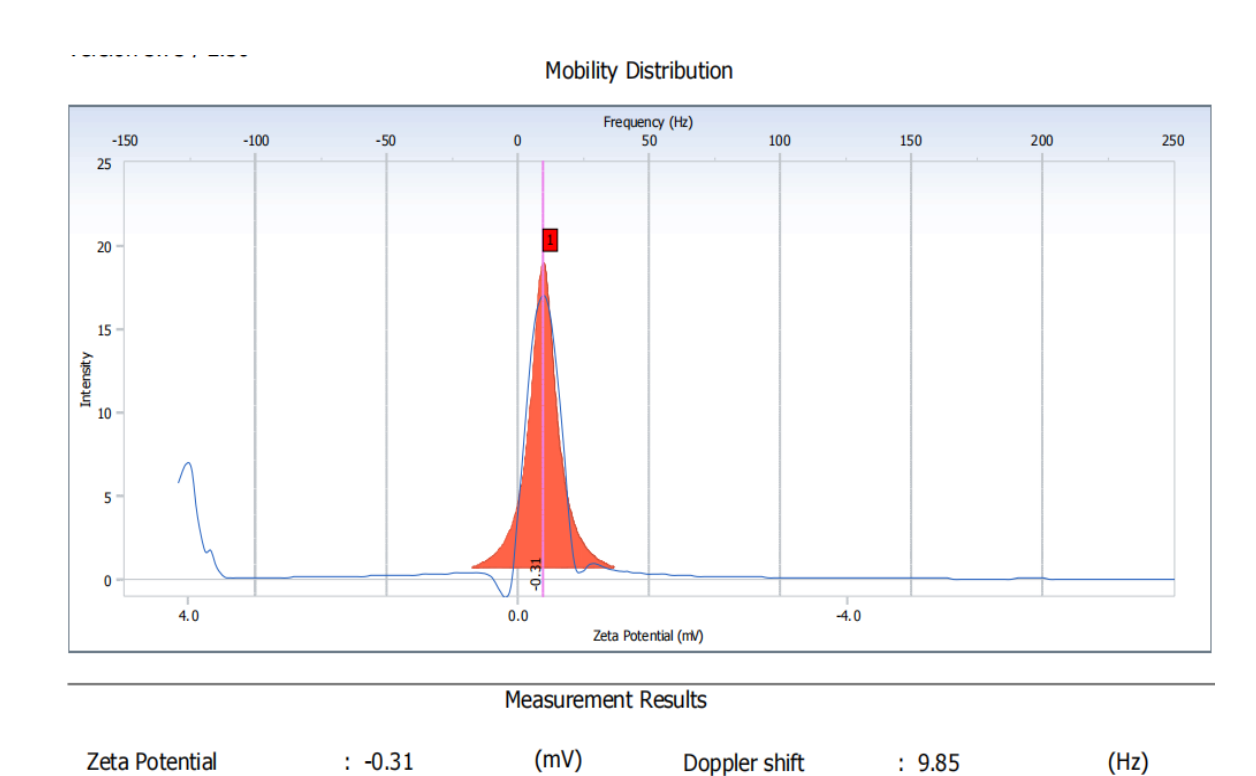


Figure 4.5: Zeta Potential for AgNPsEaqD

This indicates a higher degree of aggregation in AgNPsEETOH-D, possibly due to more adsorbed solvent molecules and ions on the nanoparticle surface. Ethanol-extracted nanoparticles may have a thicker organic layer, making them appear larger in DLS measurements.

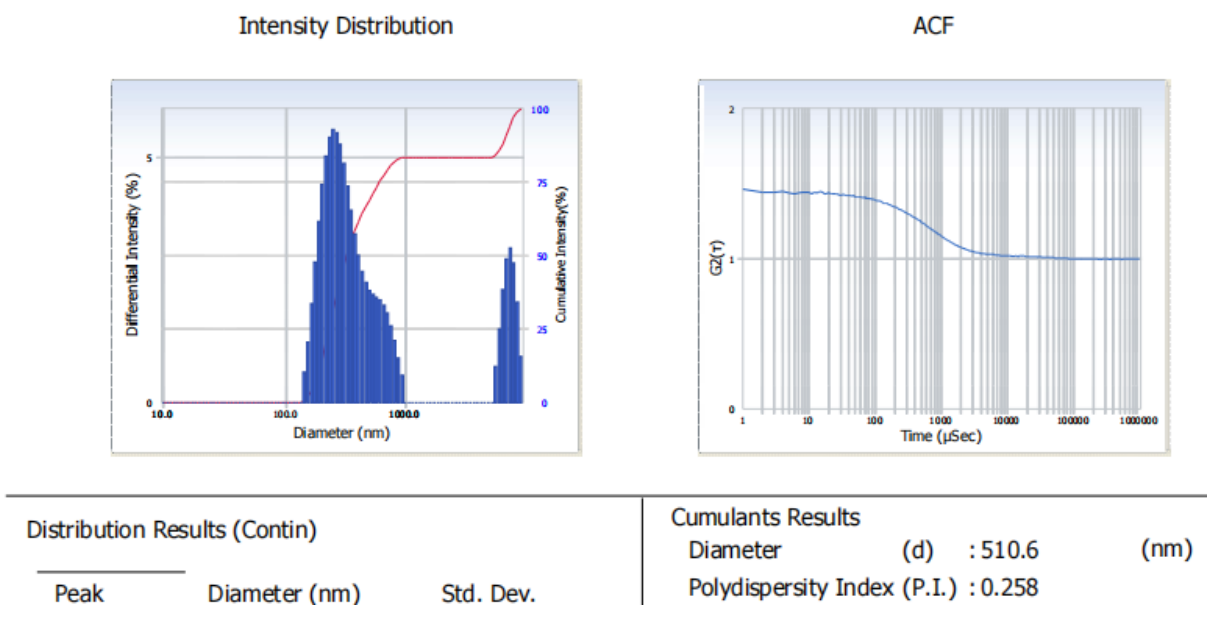


Figure 4.6: Hydrodinamic diameter, polydispersity index for AgNPsEETOHD



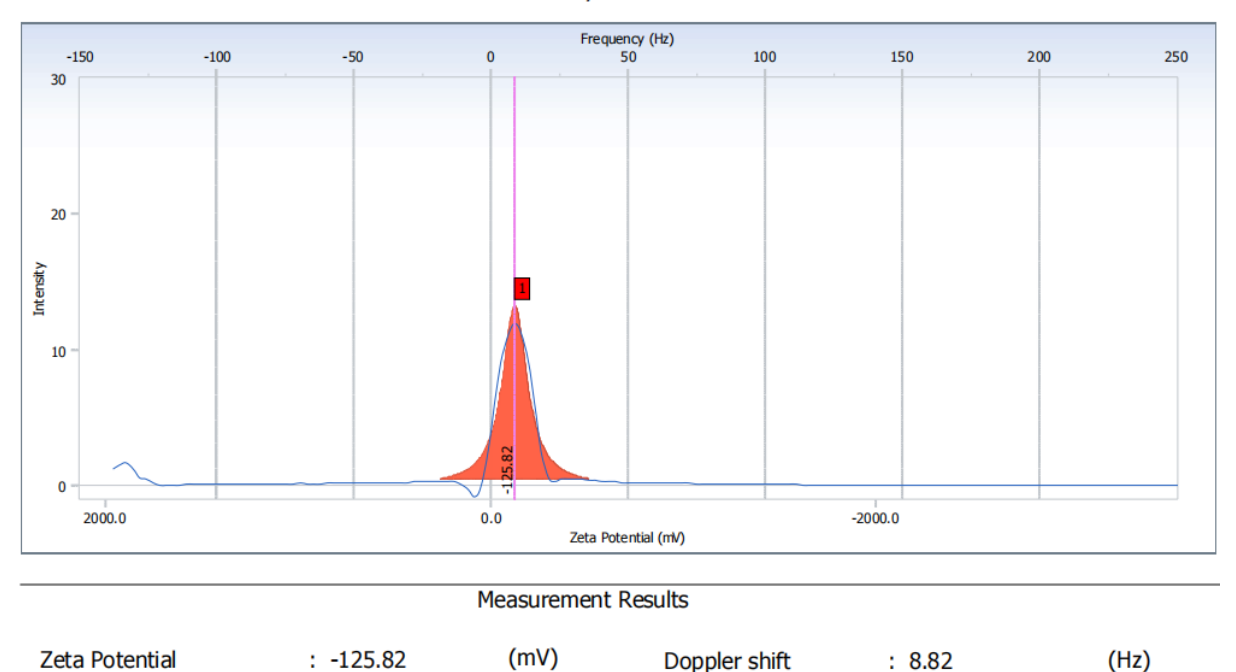
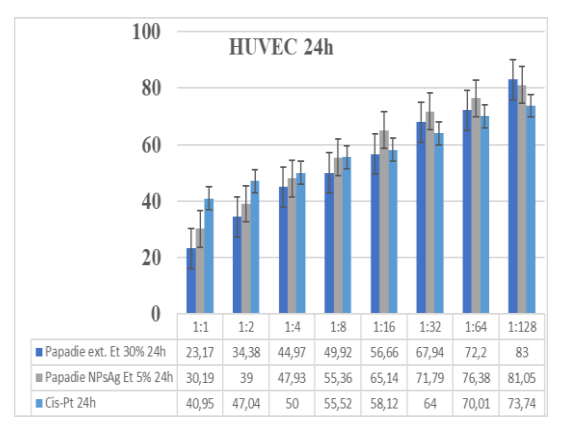


Figure 4.7: Zeta Potential for AgNPsEETOHD

This difference could influence biodistribution, cellular uptake, and cytotoxic effects. The Zeta potential of aqueous extract-derived nanoparticles was -0.31 mV (Figure 4.6), while ethanol extract-derived ones had a high negative Zeta potential of -125.82 mV (Figure 4.7), indicating increased stability.

#### **Biological Testing**

Cytotoxic effect on normal HUVEC cells



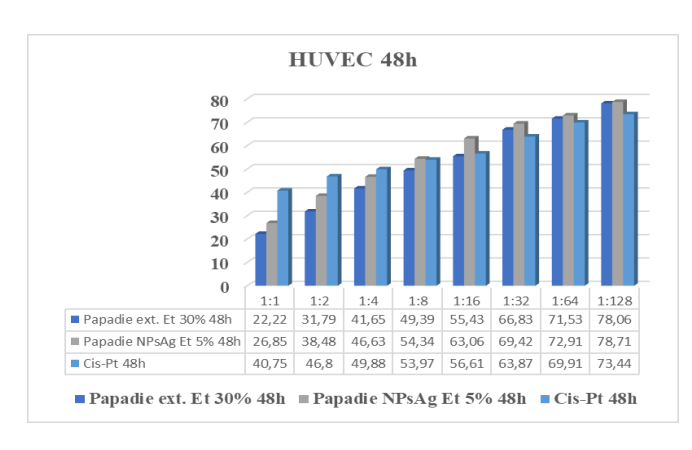


Figure 4.8:Cytotoxic effect (%) of dandelion-derived AgNPs and CisPt on normal HUVEC cells after 24 h and 48 h treatment

#### Effects of the substances on cell viability

Cis-Pt (Cisplatin) exhibits relatively high toxicity, with more pronounced effects at higher concentrations (lower dilutions). Cell viability decreases progressively as the concentration increases. NPsAg Et 5% appears to have a greater cytotoxic effect than the simple dandelion extract (Dandelion ext. Et 30%), but less than Cis-Pt, suggesting a potential moderate

activity against HUVEC cells. Dandelion ext. Et 30% shows the lowest toxicity among the three substances, having a milder impact on cell viability.

Overall, after 48 hours, toxicity tends to increase for all substances, indicating a cumulative effect over time. Both the dandelion extract and silver nanoparticles (NPsAg) maintain a similar trend, but the silver nanoparticles exhibit a more pronounced effect than the plain extract. Cis-Pt remains the most toxic substance at both time intervals.

#### Comparison Between Nanoparticles and Cis-Pt

At all dilutions, Cis-Pt is the most cytotoxic, which was expected given its nature as a potent chemotherapeutic agent.

Silver nanoparticles in dandelion extract (NPsAg) exhibit intermediate toxicity between the plain dandelion extract and Cis-Pt, suggesting their potential use as a less aggressive anticancer agent compared to Cis-Pt. The dandelion extract (Et 30%) shows the lowest toxicity, indicating a safer profile for therapeutic use or as an adjuvant.

Cis-Pt exhibits the highest toxicity toward HUVEC cells, followed by dandelion-derived NPsAg Et 5%, while dandelion extract Et 30% has the lowest cytotoxic effect. These findings suggest that silver nanoparticles combined with dandelion extract could have a less aggressive therapeutic effect than Cis-Pt, but with higher efficacy than the extract alone. Further studies are needed to better understand the mechanisms of these effects and their potential applications in medical treatments.

#### Cytotoxic Effect of Nanoparticles on the HepG2 Liver Cell Line

The graphs shown in Figures 4.9 illustrate the cell viability (%) of the HepG2 cell line (hepatocarcinoma cells) after 24 and 48 hours of treatment. The concentrations tested ranged from 1:1 to 1:128 dilutions (indicated by different colors).

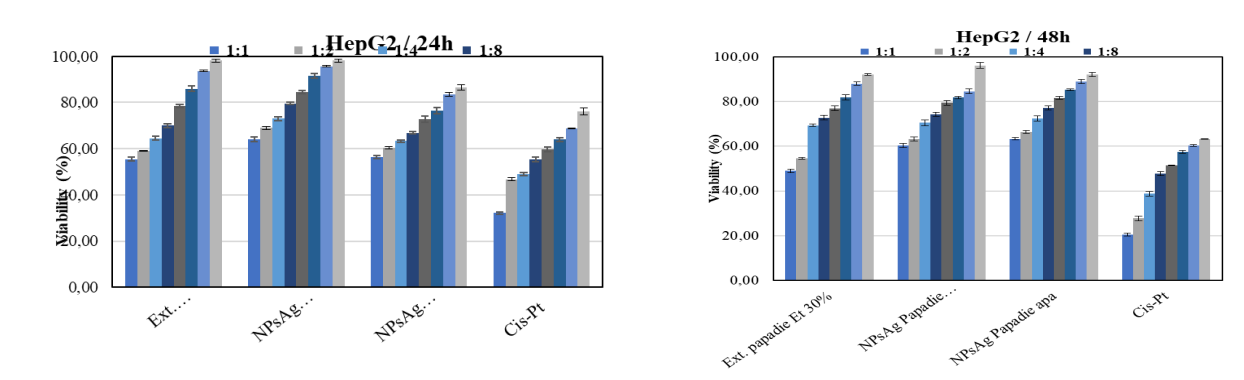


Figure 4.9: HepG2 Cell Viability (%) After 48-Hour Treatment With Nanoparticles Derived From Wormwood Compared to Cis-Pt

Based on the analysis of the results presented in the graphs from Figure 4.9, the following observations can be made:

- Under all conditions, cell viability decreases as the treatment concentration increases (from 1:128 to 1:1).
- This suggests a dose-dependent effect, where higher concentrations are more effective in reducing cell viability.
- EETOH-D and AgNPsEETOH-D exhibit lower cytotoxicity compared to AgNPsEaq-D and Cis-Pt.
- AgNPsEaq-D demonstrates greater efficacy than ethanolic extract, which may indicate better release or stability in this medium.
- Cisplatin (Cis-Pt) shows the highest cytotoxicity, with the lowest cell viability values, especially at higher concentrations.
- After 48 hours, a more pronounced decrease in cell viability is observed compared to 24 hours, indicating a cumulative treatment effect.
- Cis-Pt showed a significant reduction in viability after 48 hours compared to 24 hours, which is expected for a chemotherapeutic agent.
- AgNPsEaq-D appears to be more effective than the ethanolic extract, suggesting that nanoparticle formulation can enhance therapeutic effect.
- While Cis-Pt is the most cytotoxic, dandelion-based nanoparticle treatments may represent gentler yet effective alternatives over time.
- The effect is both dose- and time-dependent, with greater reductions in viability observed at higher concentrations and after 48 hours.

### CHAPTER V: EVALUATION OF THE ANTIPROLIFERATIVE EFFECT OF CHELIDONIUM MAJUS EXTRACT ON TUMOR CELL LINES

#### 5.1 Introduction

Greater Celandine (*Chelidonium majus*), a species belonging to the Papaveraceae family, is a medicinal plant with multiple therapeutic properties that has been used since ancient times due to its beneficial health effects. Today, it is increasingly valued in alternative medicine and phytotherapy, being recommended as an adjuvant in over 150 conditions, including neoplasms, viral infections, and dermatological disorders resistant to conventional treatments.

Academic studies have investigated the plant's chemical composition, pharmacological properties, and potential medical applications. When administered internally, *Chelidonium majus* exerts hepatoprotective effects, with tonic and regenerative actions on the liver, as well as biliary-draining, antiviral, choleretic (stimulating bile production), and cholagogue (promoting bile release) effects. Due to its broad spectrum of action, greater celandine is considered a valuable remedy in the management of various liver disorders, showing significant efficacy in the treatment of hepatitis A and B.

The mechanisms by which the active compounds in *Chelidonium majus* (chelidonine, sanguinarine, berberine) act on tumor cells include the induction of oxidative stress, disruption of the cell cycle, and activation of apoptotic pathways [223, 224]. Chelidonine, for example, has been reported to inhibit tubulin polymerization, leading to cell division arrest at the G2/M phase and thus halting the proliferation of malignant cells [225, 226]. Studies have also shown that sanguinarine acts by altering mitochondrial function, resulting in the release of cytochrome c and activation of caspases - key players in the apoptotic process [227, 228].

In addition to these direct effects on cancer cells, *Chelidonium majus* extracts have also been studied for their impact on the tumor microenvironment, including their ability to reduce angiogenesis and modulate immune responses [229, 230]. For instance, sanguinarine has been shown to inhibit endothelial growth factors, thereby preventing the formation of new blood vessels necessary for tumor development [231-233].

These mechanisms support the antitumor potential of *Chelidonium majus* and justify further investigation of this plant as an adjuvant agent in oncological therapies [234, 235].

### 5.2 In Vitro Cytotoxicity Evaluation of the Studied Compounds on Human Tumor and Normal Cell Lines

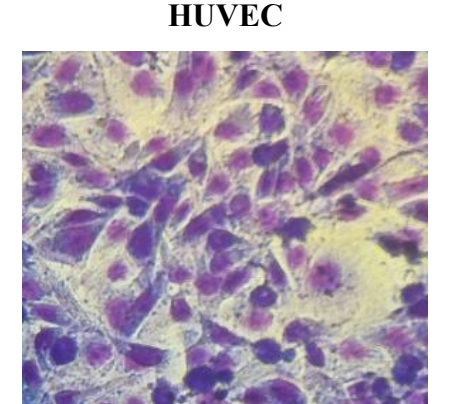
Preclinical *in vitro* studies are an essential step in determining the therapeutic potential of bioactive compounds, especially in oncology. Cytotoxicity evaluation enables the identification of specific effects on tumor cells compared to normal cells, thus contributing to the establishment of a safety and efficacy profile for future use in anticancer therapies.

#### Characteristics of Standardized Cell Lines

To investigate the cytotoxicity of the compounds studied, this research employed a standardized human tumor cell line derived from hepatic malignancies (HepG2), in comparison with normal human cells (HUVEC). These cell lines were selected due to their relevance in modeling the pathogenic mechanisms of liver cancer.

To ensure experimental standardization and result reproducibility, the cell lines used in this study were obtained from the European Collection of Authenticated Cell Cultures (ECACC), an internationally recognized reference source for authenticated cell cultures. This approach ensures the quality, genetic stability, and homogeneity of the cell lines—key factors for the validation of obtained results.

The HepG2 cell line was derived from a liver biopsy of a 15-year-old Caucasian male diagnosed with hepatocellular carcinoma. The HUVEC cell line is a normal human endothelial cell line, isolated from the vascular endothelium of an umbilical cord and immortalized in the laboratory. It was used as the normal control.



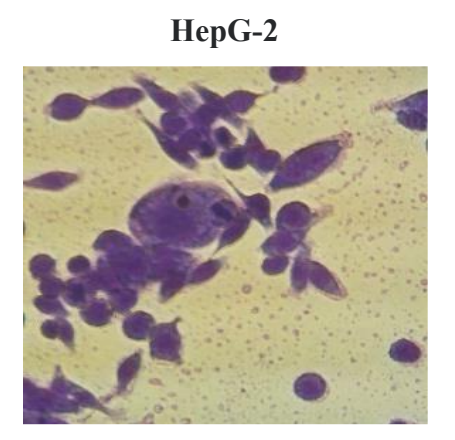


Figure 5.1: Morphological Aspects of Untreated Cell Lines Used Throughout the Studies

#### **5.3** Cultivation of Cell Lines

Cell cultures are performed and maintained in specially designated areas where a sterile environment must be ensured. The standardized cell lines used in this study were cultured and maintained according to the recommendations of the ECACC (European Collection of Cell Culture, *Fundamental Techniques in Cell Culture*).

#### Materials, Reagents, and Equipment

- Culture medium DMEM/F12 (Dulbecco's Modified Eagle Medium Gibco), washing medium Hanks' Balanced Buffer Solution (HBSS), fetal bovine serum (FBS), HEPES, L-glutamine, phosphate-buffered saline (PBS), ethylenediaminetetraacetic acid (EDTA), penicillin/streptomycin 10,000 U/10,000 μg/ml, cisplatin (CisPt) (Sigma Aldrich, St. Louis, MI, USA)
- Culture plates (flasks), 15- and 50-ml Falcon tubes, sterile pipettes of various volumes
- Laminar flow hood, incubator, refrigerated centrifuge, and microscope

#### 5.4 Evaluation of Cellular Cytotoxicity Using the Colorimetric MTS Assay

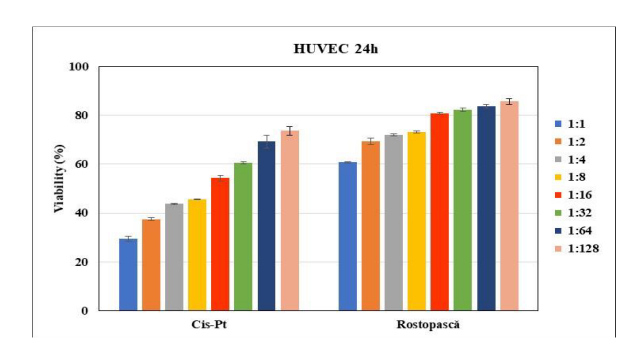
Method Principle: The cytotoxicity of the compounds used in the experiments was evaluated using the CellTiter 96® AQueous One Solution Cell Proliferation Assay (MTS) kit (Promega), a rapid and reliable colorimetric method widely used in cell proliferation and cytotoxicity assays. The MTS assay is based on the activity of mitochondrial dehydrogenases in viable cells, which catalyze the reduction of the yellow tetrazolium compound MTS into a blue-violet formazan product that is soluble in the culture medium. The amount of formazan produced is directly proportional to the enzymatic activity of viable cells and, therefore, to their number. The absorbance of the formazan solution is measured spectrophotometrically at 490 nm, allowing for accurate quantification of cell viability.

#### 5.5 Evaluation of the Cellular Cytotoxicity of the Studied Compounds

The studies were conducted to assess the effects of specific compounds on human HepG2 tumor cells (hepatic adenocarcinoma), in comparison with the normal HUVEC cell line (human umbilical vein endothelial cells). Cisplatin (CisPt), a commonly used cytostatic agent in liver cancer treatment, was employed as a positive control. The cell lines were exposed to various concentrations of the tested compounds for time intervals of 24 and 48 hours.

To determine the optimal concentration, dose–response curves were generated for both the studied extract and the cytostatic agent, using serial dilutions ranging from 1:1 to 1:128. These curves revealed a direct dose-dependent relationship between compound concentration and cell viability. The results can contribute to optimizing the doses for future studies and to developing effective therapeutic strategies aimed at maximizing antitumor efficacy while minimizing toxicity to normal cells.

HUVEC cells were treated with different concentrations of Chelidonium majus extract and compared with cisplatin over 24 and 48 hours (Figure 5.4).



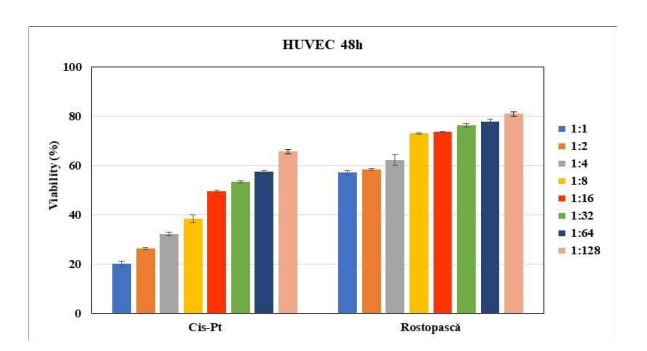
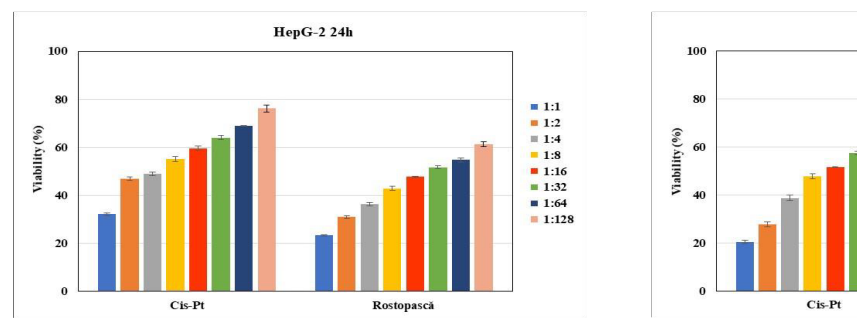


Figure 5.3: Effect of Treatment on Normal Endothelial HUVEC Cells at 24 and 48 Hours

Viability assays showed that, at 24 hours post-treatment, *Chelidonium majus* extract affected the viability of normal HUVEC cells only at 1:1 and 1:2 dilutions. After 48 hours of treatment, cell viability was affected at 1:1, 1:2, and 1:4 dilutions.

Human hepatic tumor cells (HepG2) were treated with various concentrations of *Chelidonium majus* extract, in comparison with cisplatin, for 24 and 48 hours (Figure 5.3).



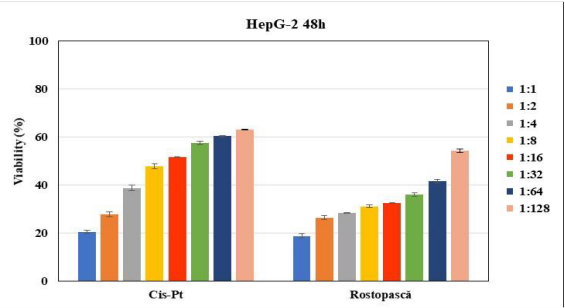


Figure 5.4: Antiproliferative Effect in HepG2 Liver Tumor Cells at 24 and 48 Hours

Treatment of HepG2 liver tumor cells for 24 hours with Chelidonium majus extract showed that, at a 1:8 dilution, it eliminated 58% of the tumor cells, compared to cisplatin, which killed 42% at the same dilution.

Analysis of viability data following treatment of the HepG2 tumor cell line with Chelidonium majus extract revealed that, after 24 hours, the extract demonstrated greater efficacy than cisplatin. After 48 hours of treatment, Chelidonium majus exhibited an even more pronounced antitumor effect than the cytostatic agent used (CisPt).

The use of plant extracts as modulators of the cellular response to conventional treatments (chemotherapy) opens up new opportunities and perspectives in cancer therapy. Numerous studies have shown that secondary metabolites derived from medicinal plants, microorganisms, or other natural sources can act synergistically with chemotherapeutic agents, enhancing their efficacy while reducing associated side effects.

# CHAPTER VI: ANTIOXIDANT AND ANTIBACTERIAL ACTIVITY OF EXTRACTS FROM *CLEMATIS HERBA*, *MELISSAE FOLIUM*, *TARAXACI HERBA*, AND *SILYBII FRUCTUS*

#### 6.1. Quantitative Determination of Polyphenolic Compounds

Polyphenols are a class of organic chemical compounds found in plants, characterized by diverse chemical structures containing phenolic groups. They exhibit multiple pharmacological activities, including antioxidants, anti-inflammatory, and cardioprotective effects.

#### 6.1.1. Materials and Method

The quantitative determination of polyphenols was performed using the Singleton spectrophotometric method, based on the reaction of total polyphenols with the Folin–Ciocalteu reagent. The absorbance of the resulting-colored solution was measured at a wavelength of 765 nm, using gallic acid as a standard.

For the extraction of phenolic compounds, dried plant materials (*Clematis herba*, *Melissae folium*, *Taraxaci herba*, *Silybii fructus*) were used to prepare 1% (w/w) ethanolic extracts (50%). The extraction procedure consisted of refluxing in a water bath for 30 minutes, followed by filtration and volume adjustment in a graduated flask.

The Singleton spectrophotometric method using the Folin–Ciocalteu reagent [236] proved to be precise and reproducible for the determination of polyphenols in the ethanolic extracts of the analyzed plant materials. The well-defined calibration curve and the high determination coefficient confirm the method's validity for analyzing phenolic compounds.

#### 6.1.2. Results and Discussion

The results obtained from the determination of total polyphenol content, expressed as milligrams of gallic acid equivalents per gram of dry plant material (mg GAE/g dry plant material), revealed significant variations among the analyzed plant species. The highest concentrations of polyphenols were observed in *Melissa officinalis* (31.6 mg GAE/g dry plant material) and *Clematis vitalba* (31.26 mg GAE/g), while *Taraxacum officinale* (15.7 mg GAE/g) and *Silybum marianum* (15.5 mg GAE/g) showed considerably lower values.

Due to their high polyphenol content, *Melissa officinalis* and *Clematis vitalba* exhibit significant pharmacological potential, particularly for applications aimed at preventing diseases associated with oxidative stress.

#### **6.2.** Antioxidant Activity

#### 6.2.1. Materials and Method

The antioxidant capacity of various compounds plays a key role in assessing their potential health benefits. One of the most commonly used methods for determining antioxidant activity is the DPPH assay, which is based on the ability of antioxidants to neutralize free radicals. This method involves the preparation of a stable DPPH solution in methanol, characterized by an intense violet color due to the presence of an unpaired electron. In the presence of antioxidant compounds, DPPH is reduced through electron or hydrogen atom transfer, resulting in the formation of a pale yellow compound [237, 238].

#### 6.2.3. Results and Discussion

The antioxidant activity of the tested plant extracts, determined using the DPPH free radical scavenging method, showed significant variation in their capacities:

- Clematis vitalba (88.13%) exhibited the highest antioxidant activity among the tested plants, with a very strong free radical absorption capacity. This suggests that it contains a high concentration of active antioxidant compounds such as flavonoids, polyphenols, or other bioactive phytochemicals.
- *Melissa officinalis* (68.73%) showed a relatively high antioxidant capacity, though lower than that of *Clematis vitalba*. This plant is known for its high content of rosmarinic acid and other phenolic compounds, which likely contribute to its ability to neutralize free radicals.
- *Taraxacum officinale* (27.22%) demonstrated moderate antioxidant activity.
- Silybum marianum (21.41%) showed the lowest antioxidant activity among the tested plants. Although Silybum marianum is known for its flavonolignans (such as silymarin), which possess antioxidant properties, its radical scavenging potential in this assay appears to be less effective compared to the other species.

#### 6.3. Antimicrobial Activity

The aim of this study was to investigate the antimicrobial activity of *Taraxacum officinale* (tincture) and *Chelidonium majus* (tincture) extracts using a multidimensional approach that included qualitative and quantitative methods as well as biofilm activity analysis. The in vitro antibiofilm properties of *Taraxacum officinale* and *Chelidonium majus* plant extracts were evaluated by assessing their ability to inhibit microbial biofilm formation on inert surfaces. For this evaluation, the crystal violet 1% microtiter plate assay was used, which allows quantification of biofilm formation in the presence of various extract concentrations.

The qualitative assessment of the antimicrobial activity of *Taraxacum officinale* extract revealed inhibition of microbial growth against *Enterococcus faecalis* ATCC 29212 (9 mm inhibition zone), *Pseudomonas aeruginosa* ATCC 27853 (8 mm with weak microbial growth within the inhibition zone), and *Candida albicans* ATCC 10231 (8 mm with numerous colonies inside the inhibition zone). In contrast, *Staphylococcus aureus* ATCC 25923 and *Escherichia coli* showed resistance to the extract, with no inhibition of microbial growth.

The *Chelidonium majus* extract demonstrated antimicrobial activity by inhibiting *Candida albicans* ATCC 10231 with a 7 mm inhibition zone. Bacterial growth was also inhibited in Escherichia coli ATCC 25922 (7 mm inhibition zone) and Enterococcus faecalis ATCC 29212 (11 mm inhibition zone). However, the extract showed no effect against *Staphylococcus aureus* ATCC 25923 and *Pseudomonas aeruginosa* ATCC 27853.

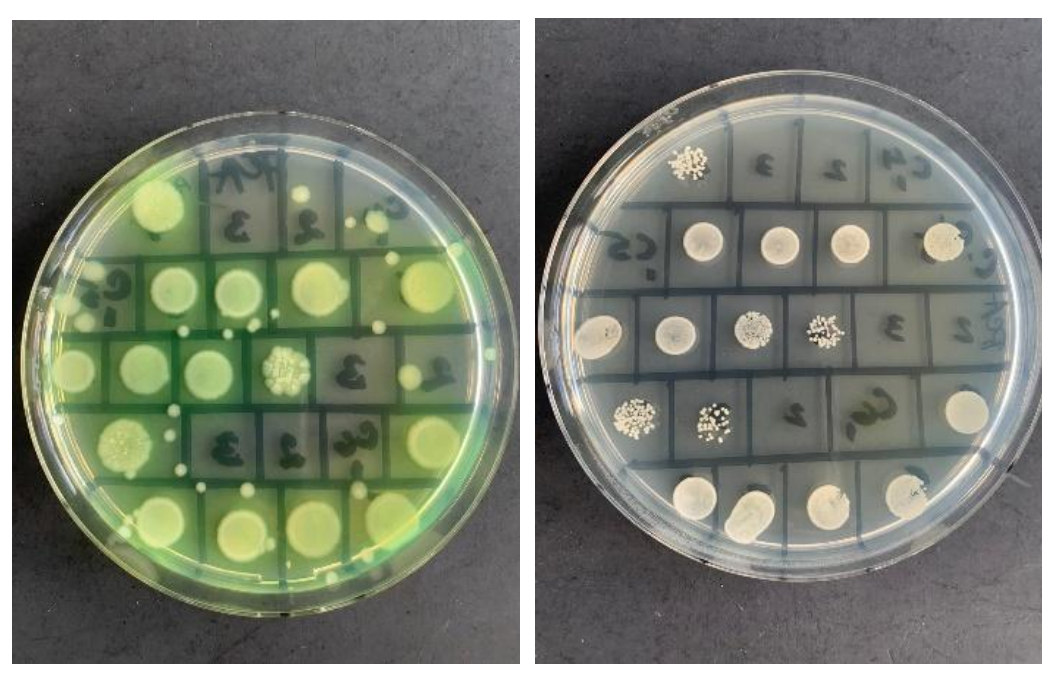


Figure 6.1: Results of Antimicrobial Activity Testing:

Agar medium inoculated with droplets from 96-well microplates containing strains of Staphylococcus aureus, Enterococcus faecalis, Escherichia coli, Pseudomonas aeruginosa, and Candida albicans, after incubation for 18–24 hours at 37°C.

After incubating the ELISA microplates for 24 hours, crystal violet absorbance was measured spectrophotometrically at 492 nm to determine the effectiveness of each extract in preventing biofilm development. The minimum concentration of each extract required to inhibit biofilm formation was determined by comparing absorbance values with those of the positive control. The results were analyzed to identify differences in the effectiveness of the extracts against Gram-positive bacteria, Gram-negative bacteria, and fungi.

Based on the experimental data, the potential use of these plant extracts in combating biofilm-associated infections - known for their high resistance to conventional antimicrobial treatments - was assessed.

#### 6.4. Conclusions

The pronounced antioxidant activity of Melissa officinalis and Clematis vitalba can be correlated with their high polyphenol content. Consequently, these species may possess enhanced pharmacological and nutritional potential, particularly in applications aimed at preventing diseases associated with oxidative stress.

The qualitative assessment of antimicrobial activity demonstrated that the plant extracts inhibited the growth and development of the tested microbial strains. The results are promising and support the need for further research into the biochemical properties of these extracts, with the aim of developing effective strategies for combating bacterial and fungal infections in humans.

#### CHAPTER VII: *IN VITRO* SYNERGISM BETWEEN GREEN-SYNTHESIZED NANOPARTICLES AND NEXT-GENERATION ANTITUMOR DRUGS ON CELL LINES

#### 7.1 Introduction

The main objective of this study is to investigate the synergistic effects between nanoparticles derived from *Clematis vitalba* and *Taraxacum officinale* when used in combination with anticancer drugs for hepatocellular carcinoma.

Previous studies have shown that dandelion extracts and biogenic nanoparticles synthesized from them exhibit significant antitumor activity, comparable to cisplatin and doxorubicin - two of the most widely used chemotherapeutic agents in breast, colorectal, and hepatocellular cancers. In this study, the synthesized nanoparticles were tested in combination with antitumor drugs used for liver cancer treatment. Sunitinib and Imatinib were selected as reference agents, both being tyrosine kinase inhibitors with strong antitumor activity in various cancers, including advanced or metastatic hepatocellular carcinoma.

We analyzed the combined effect of these therapies on viability, proliferation, and apoptotic mechanisms in hepatocarcinoma cells, and compared the results to those obtained in normal liver cells. Through this research, we aim to assess the improvement in therapeutic efficacy and the reduction of side effects, opening new perspectives for innovative treatments in liver cancer.

#### 7.2 Experimental Methods

#### 7.2.1 Biosynthesis of Nanoparticles Using Plant Extracts

The procedure for obtaining therapeutic nanosystems is based on the principles of green synthesis (*Green Chemistry Principles*) for producing bio-nanoparticles using various alcoholic or aqueous plant extracts. This method is safe, simple, cost-effective, non-toxic, environmentally friendly, and offers the advantages of reproducibility and sustainability, with the final nanoparticle forms often being much more stable.

#### 7.2.2. Physicochemical Characterization of Biosynthesized Nanoparticles from Plant Extracts

The physicochemical characterization of nanoparticles obtained through green synthesis methods was performed using various modern techniques to evaluate their size, shape, and surface morphology.

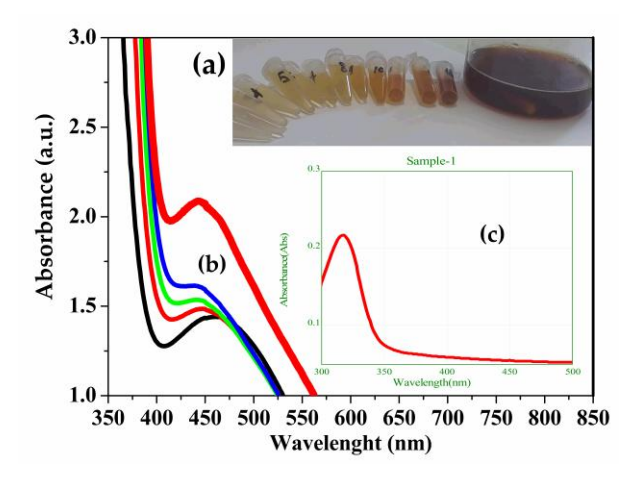
The optical absorption properties of AgNPs were assessed using a UV-Vis spectrophotometer with a photodiode array detector, model U-0080D (Hitachi, Japan). The hydrodynamic diameter and surface charge of the silver nanoparticles were analyzed using a

Beckman Coulter Delsa Nano C instrument, equipped with dynamic light scattering (DLS) and electrophoretic light scattering (ELS) capabilities.

Time-dependent fluctuations in laser light intensity were generated by illuminating the nanoparticles with a dual 30 mW laser diode. Morphological analysis of the nanoparticles was performed using a field-emission scanning electron microscope (FE-SEM), model Nova NanoSEM 630, operating at an accelerating voltage of 10.0 kV and a magnification of up to 2,000,000x.

#### Monitoring of Biosynthesized Nanoparticles from Plant Extracts by UV-Vis Absorption Spectroscopy

Figures 7.1 and 7.2 show the spectral characterization, performed using UV-Vis absorption spectrometry, of the samples recorded during the synthesis of silver nanoparticles (AgNPs) from Melissa officinalis (ME AgNPs) and Clematis vitalba (CVE AgNPs), respectively.



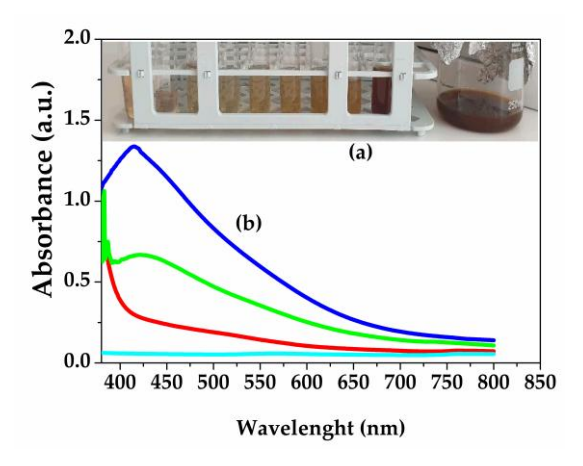


Figure 7.1: (a) Color change of the solution from reddishbrown to dark brown as a result of the bioreduction of silver by Melissa officinalis extract; (b) UV–Vis spectra of ME AgNP samples obtained through time-dependent reduction using Melissa officinalis extract; (c) UV–Vis spectra of the aqueous AgNO<sub>3</sub> 0.5 mM solution.

Figure 7.2: (a) Color change of the solution from reddishbrown to dark brown as a result of the bioreduction of silver by Clematis vitalba extract; (b) UV–Vis spectra of CVE AgNP samples obtained through time-dependent reduction using Clematis vitalba extract.

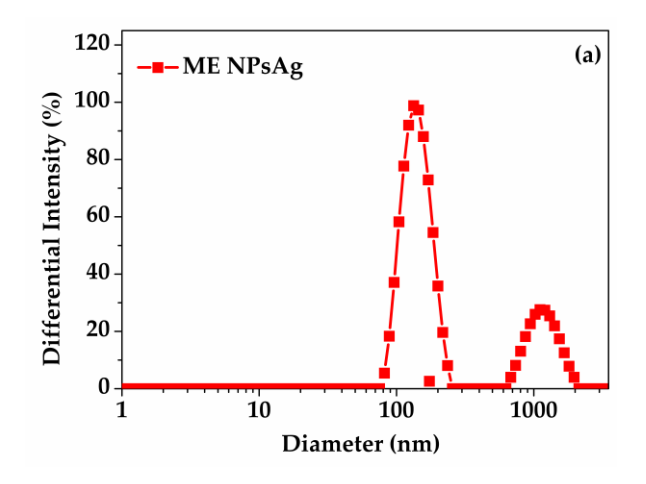
As shown in Figures 7.1(a) and 7.2(a), a color change from reddish-brown to dark brown was observed after mixing the AgNO<sub>3</sub> solution with the plant extracts. This color change was attributed to the formation of silver nanoparticles. Additionally, nanoparticle formation was confirmed by the appearance of absorption maxima between 400 and 460 nm in both syntheses. Figure 7.1(b) illustrates an initial maximum absorption at 453 nm, which then shifted to a lower value and stabilized at 440 nm after 30 minutes, indicating the formation of silver nanoparticles biosynthesized from Melissa officinalis extract (ME AgNPs).

Thus, the silver nanoparticles biosynthesized from *Clematis vitalba* were found to be smaller in size compared to those derived from *Melissa officinalis*, even though a slightly larger

volume of plant extract was used. The ratio between silver nitrate solution and *Clematis* extract was 2:1 (v:v).

#### Evaluation of Nanoparticles Using DLS, ELS, and SEM Techniques

In this study, dynamic light scattering (DLS), electrophoretic light scattering (ELS), and scanning electron microscopy (SEM) were employed to analyze the interactions of two types of biogenic silver nanoparticles in their final colloidal forms post-biosynthesis. Although the plant extracts were filtered prior to being used in the biosynthesis of nanoparticles, the nanoparticles themselves were not purified, which may have led to the presence of larger extract particles remaining alongside the nanoparticles.



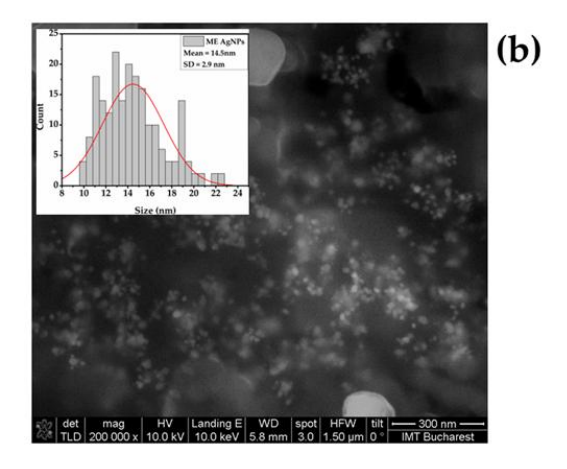


Figure 7.3: (a) DLS Measurements for ME AgNPs

Figure 7.3: (b) SEM Images for ME

Figure 7.3 (a) illustrates the size distributions by intensity for silver nanoparticles synthesized using *Melissa officinalis* extract (ME AgNPs). The size distribution profile revealed two particle populations: a broad distribution ranging from 75 nm to 255 nm, centered at 143 nm, and a larger size population centered at 1108 nm, the latter being attributed to larger particles from the *Melissa officinalis* extract.

The SEM image of the colloidal solution containing both nanoparticles and *Melissa* officinalis extract (Figure 7.3 (b)), after dehydration, shows that the nanoparticles were considerably smaller than those measured by the DLS technique, suggesting they were coated with negatively charged compounds from the plant extract. This observation is supported by the stable negative zeta potential of -12.2 mV for the nanoparticles in *Melissa officinalis* extract, as shown in Figure 7.3 (c).

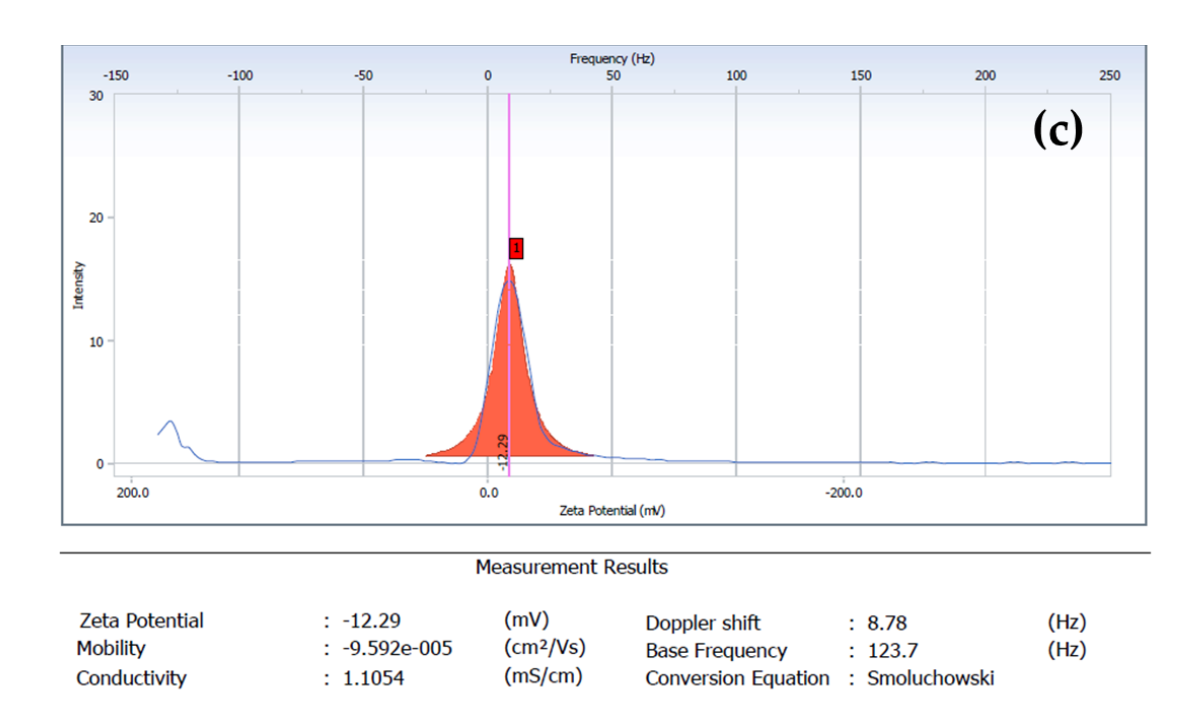
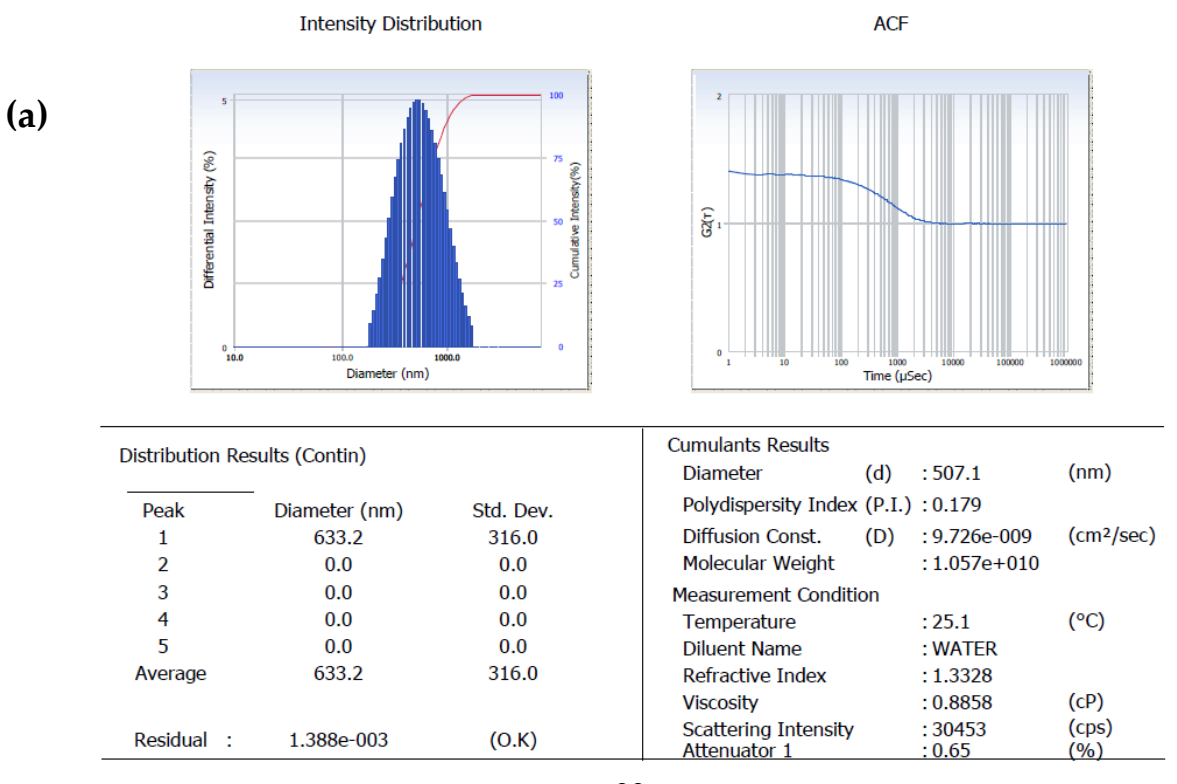
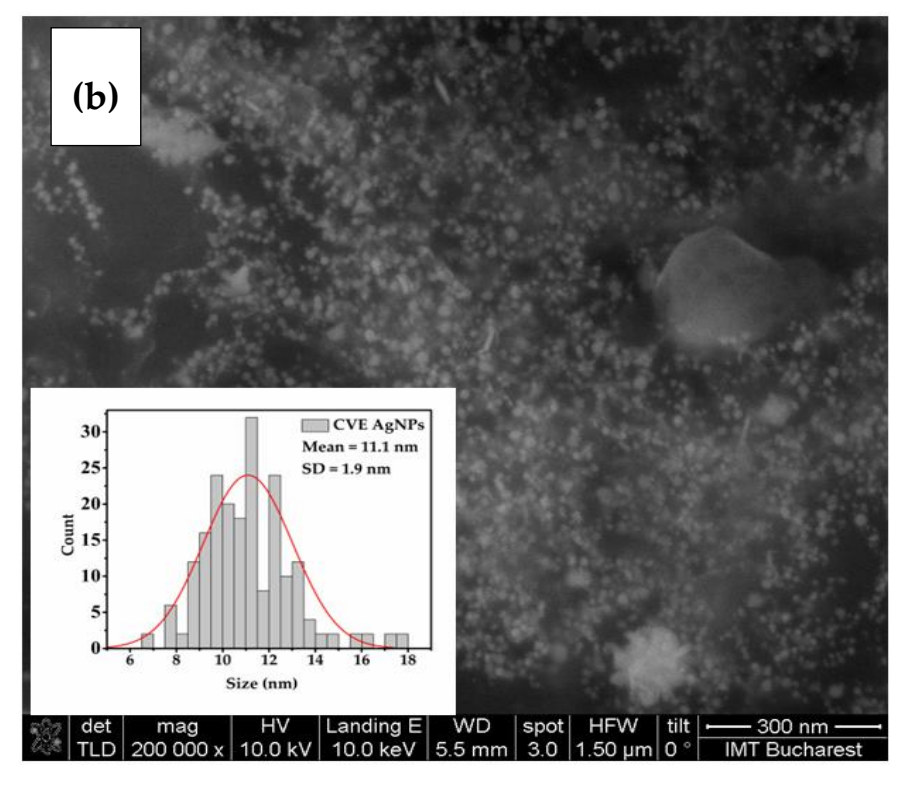


Figure 7.3: (c) Zeta Potential (mV) of ME AgNPss.

For the nanoparticles synthesized from *Clematis vitalba*, their very small size led to the onset of aggregation, confirmed by an increase in the hydrodynamic diameter, which consequently resulted in a negative but very low zeta potential, indicating instability in the resulting nanoparticle solution.

Figure 7.4 (a–c) shows the hydrodynamic diameter, SEM image with inserted histogram, and zeta potential recorded for the silver nanoparticles derived from *Clematis vitalba* extract (CVE AgNPs).





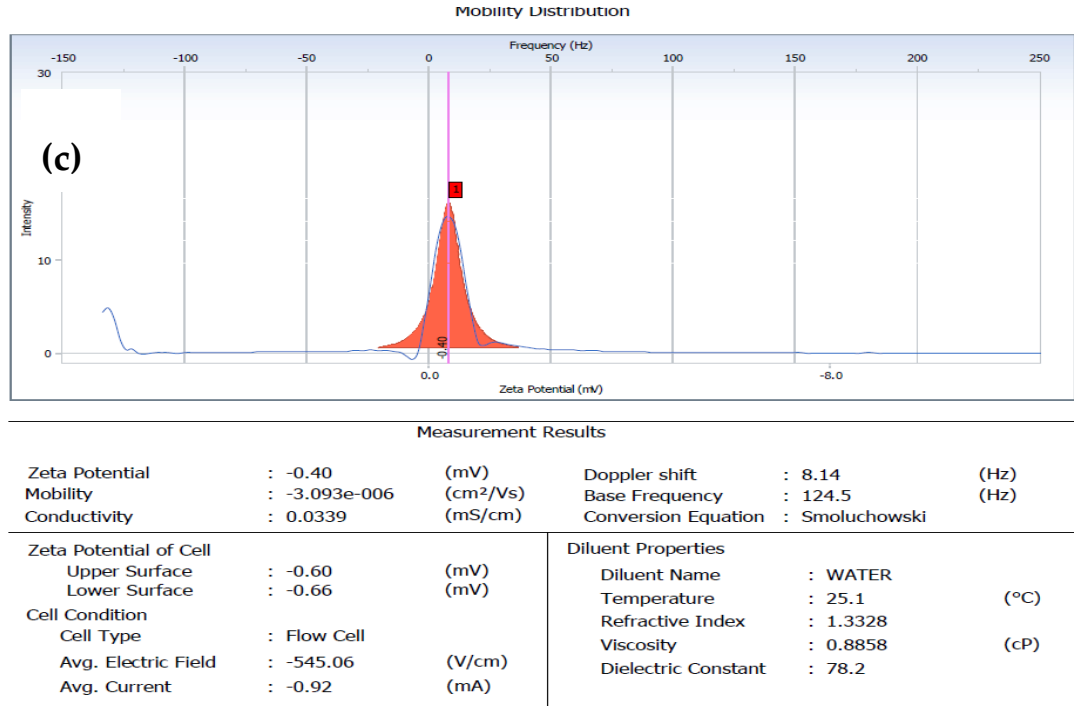


Figure 7.4: (a) DLS measurements for CVE AgNPs; (b) SEM images for CVE AgNPs; (c) Zeta potential (mV) determination for CVE AgNPs

#### 7.3 In Vitro Antitumor Testing

#### 7.3.1 Taraxacum extractum (TE)

Figures 7.5(a) and 7.5(b) illustrate cell viability in the treatment of HepG2 liver cancer cell line with dandelion-derived samples after 24 & 48 hours, respectively. Different treatment concentrations were applied to the HepG2 hepatic tumor cell line. The variation in values suggests a differential efficacy of the treatment depending on concentration and exposure time.

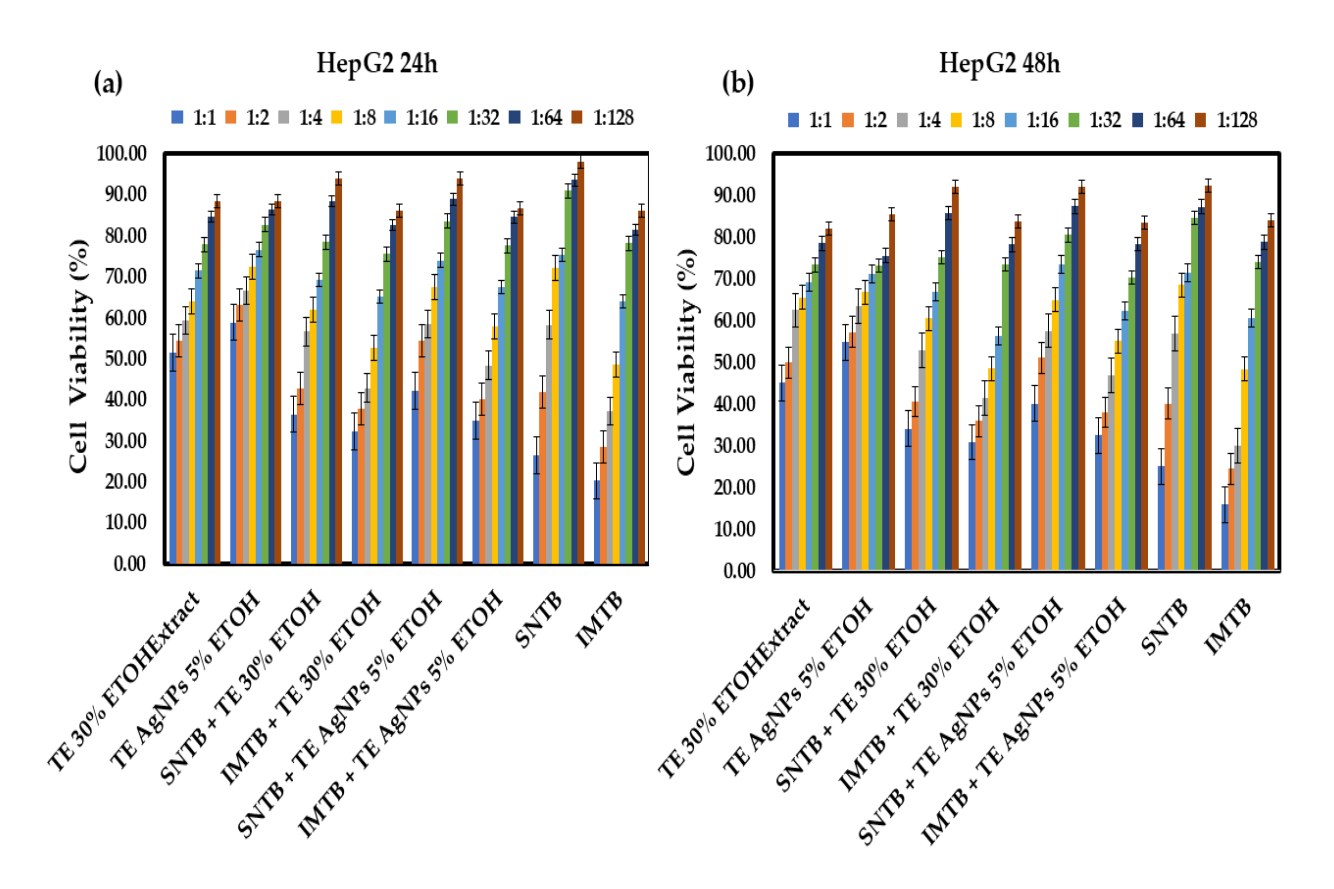


Figure 7.5: Cell viability (%) of HepG2 cell lines after: (a) 24 hours of treatment with various dilutions of Taraxacum-based extract samples and the chemotherapeutic drugs Sunitinib and Imatinib; (b) the same measurements after 48 hours of treatment.

At 24 hours, each treatment shows a range of values with varying intensities. The antitumor activity of all samples is evident, particularly at specific dilution thresholds. The chemotherapeutic drugs demonstrate the strongest effect on hepatic tumor cells at these concentrations. The combination of 30% ethanolic dandelion extract exhibits nearly the same cytotoxic effect as the combination with dandelion-derived silver nanoparticles (TE AgNPs). However, the addition of nanoparticles does not enhance the antitumor effect on the HepG2 liver cell line after 24 hours.

After 48 hours, the treatments appear to follow a similar pattern; however, lower dilutions become more effective, progressively demonstrating cytotoxicity against tumor cells over time. Nevertheless, the samples containing silver nanoparticles do not show any improvement in antitumor efficacy (p > 0.05), suggesting that this combination is less effective than conventional chemotherapeutic agents.

Although the results obtained for the dandelion-based samples, compared to control groups (Sunitinib and Imatinib), were not statistically significant, it can be stated that the viability of hepatic tumor cells in the groups treated with TE AgNPs and synthetic drugs is very similar to that observed in the control groups. Additionally, the toxic effects of the dandelion-derived samples on the normal HUVEC cell line were investigated. While a clear cytotoxic effect on

hepatic tumor cells was observed at both 24 and 48 hours, it is preferable for these samples not to exert toxic effects on normal HUVEC cells.

A cytotoxic effect of the dandelion-derived samples was also observed in HUVEC cells, similar to the chemotherapeutic drugs. However, a slight improvement in cell viability was noted when Sunitinib was administered in combination with silver nanoparticles, indicating that the toxicity of Sunitinib on endothelial cells is mitigated by the addition of silver nanoparticles. Silver nanoparticles biosynthesized from dandelion have been documented in several studies to possess antioxidant effects, thereby protecting cells from oxidative stress induced by Sunitinib.

#### 7.3.2 Clematis vitalbae extractum (CVE)

Figures 7.6(a) and 7.6(b) illustrate cell viability following treatment of HepG2 cells with samples derived from Clematis vitalba. Among the three extracts analyzed, Clematis vitalba demonstrated the most pronounced cytotoxicity against the HepG2 liver cell line.

This cytotoxic effect persisted for both 24 and 48 hours, even at the highest dilution of 1:128. Moreover, when combined with silver nanoparticles (CVE AgNPs), the cytotoxicity was reduced but remained statistically significant (p < 0.05) at the first two dilutions (1:1 and 1:2).

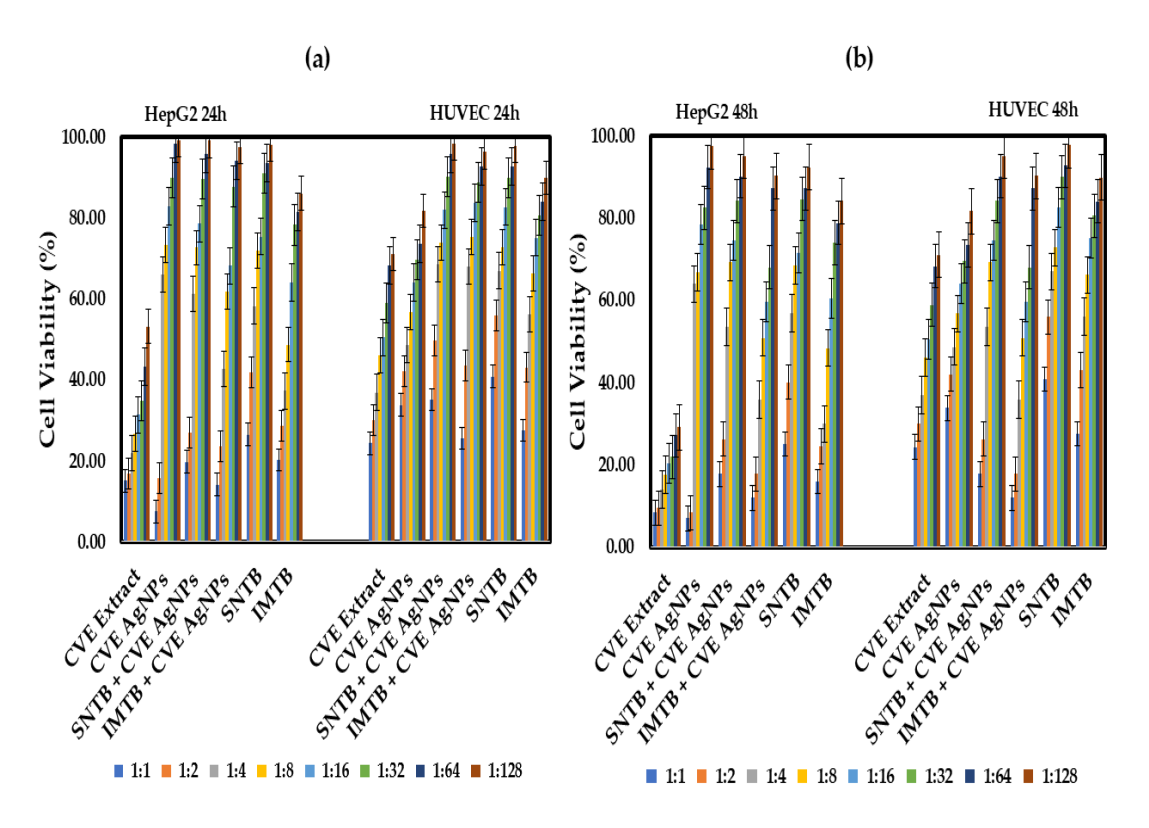


Figure 7.6: Cell viability (%) after: (a) 24 hours of treatment of HepG2 and HUVEC cells with Clematis vitalba extract-based samples, and (b) 48 hours of treatment of HepG2 and HUVEC cells with Clematis vitalba extract-based samples.

It is important to emphasize that the cytotoxicity of the Clematis vitalba extract on HUVEC cells was observed at a lower magnitude. However, normal cell proliferation was not affected at higher dilutions - dilutions at which the extract effectively inhibited the proliferation of hepatocellular carcinoma cells.

A further noteworthy finding was that both the extract and its derived formulations, including nanoparticles and their combinations with drugs, exhibited stronger antitumor effects compared to the administration of synthetic drugs alone, particularly at dilutions of 1:2 or 1:4.

All treatment groups were separately compared to the two control groups (sunitinib – SNTB and imatinib – IMTB), and the statistical analysis confirmed our observations. Statistically significant differences (p < 0.05) were found in the post-hoc tests as follows: CVE 1:1 vs SNTB (p = 0.004), CVE 1:2 vs SNTB (p = 0.010), CVE 1:4 vs SNTB (p = 0.035), CVE AgNPs 1:1 vs SNTB (p = 0.005), CVE AgNPs 1:2 vs SNTB (p = 0.005), SNTB + CVE AgNPs 1:1 vs SNTB (p = 0.000), and SNTB + CVE AgNPs 1:2 vs SNTB (p = 0.018).

These results clearly demonstrate that both CVE (at 1:1, 1:2, and 1:4 dilutions) and AgNPs CVE (at 1:1 and 1:2) induced a significant reduction in HepG2 tumor cell viability compared to the synthetic chemotherapeutic drug sunitinib.

Overall, the findings highlight that nanoparticle-based formulations significantly enhance drug potency and synergistic potential. CVE-NP-based combinations exhibited the most consistent synergy, particularly with SNTB and IMTB. Moreover, the data show that Sunitinib-based combinations tend to exhibit dose-dependent effects, whereas Imatinib-based combinations maintain more stable synergy across multiple levels of inhibition.

#### 7.4. Conclusions

In conclusion, it was confirmed that the concomitant administration of sunitinib or imatinib with silver nanoparticles biosynthesized from plant extracts improved the viability of normal HUVEC cells, suggesting a protective effect against the toxicity of synthetic drugs.

All three extracts demonstrated marked anti-cutting potential, with their combination with silver nanoparticles yielding varying degrees of success. The combination of Taraxacum officinale extract (TE) with AgNPs showed weaker results compared to the 30% ethanolic extract when applied to HepG2 cell lines, with no significant impact on their viability.

Moreover, Taraxacum-derived samples exhibited cytotoxic effects on normal HUVEC cells, similar to those observed with reference chemotherapeutic agents.

# CHAPTER VIII: MOLECULAR DOCKING STUDY OF BIOACTIVE COMPOUNDS FROM MEDICINAL PLANTS AND TYROSINE KINASE INHIBITORS

Molecular docking is a computational method that allows the determination of how a molecule - usually referred to as a ligand - binds to a macromolecule known as a receptor.

#### 8.1. Preparation and Characterization of Receptor Structures

In order to perform molecular docking, the structures of both receptors and ligands must first be prepared. The following section outlines the preparatory steps prior to docking, followed by the actual docking procedure.

The three-dimensional structures of the apelin receptor, the beta-2 adrenoceptor, and the A2B adenosine receptor—derived from X-ray crystallography—were retrieved from the Protein Data Bank. Their corresponding identification codes (PDB IDs) are: 7SUS [247], 4LDE [248] and 8HDO [249], respectively. The apelin receptor (7SUS) consists of a single chain containing 347 amino acid residues and one zinc ion. Its secondary structure analyzed using the PDBsum platform [250] is shown in Figure 8.1. It includes 14  $\alpha$ -helices, as well as  $\beta$ - and  $\gamma$ -sheet structures.

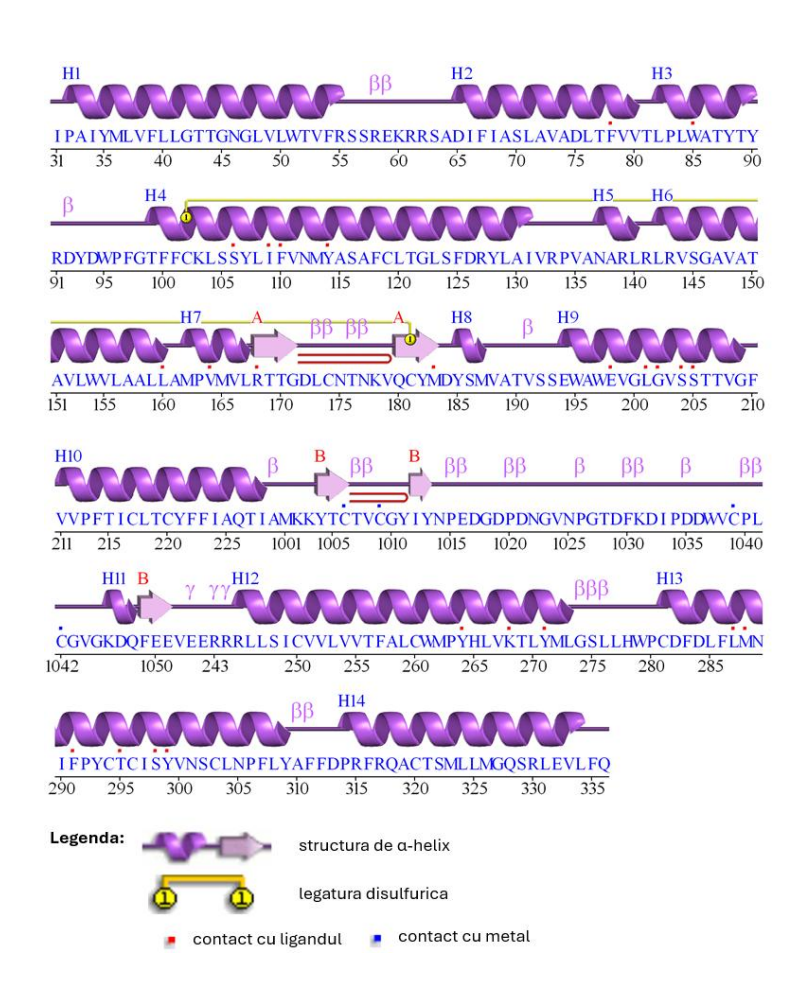


Figure 8.1: The secondary structure of the apelin receptor (7SUS) generated using the PDBsum platform

The four main binding sites have volumes of 4954.50 Å<sup>3</sup> (red region in Figure 8.2), 2025.42 Å<sup>3</sup> (purple), 1161.00 Å<sup>3</sup> (yellow), and 941.62 Å<sup>3</sup> (red).

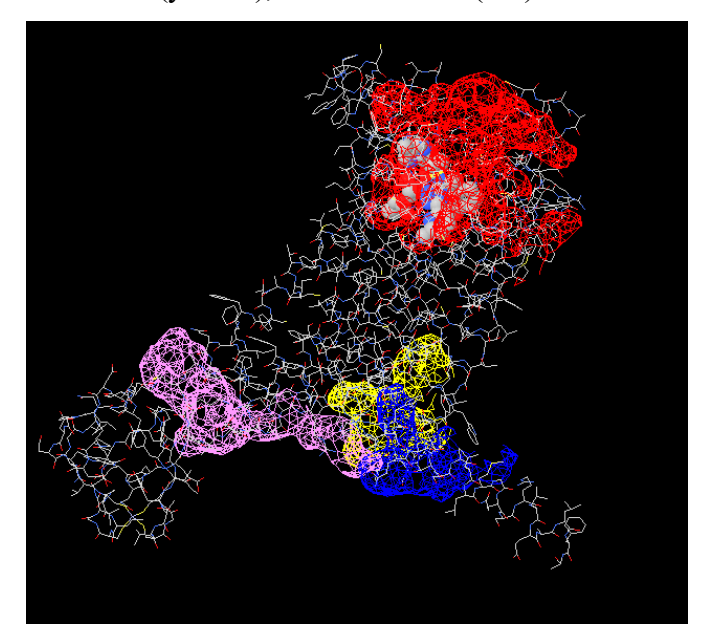


Figure 8.2: The main binding sites of the apelin receptor (7SUS) generated using the PDBsum platform.

The four main binding sites of the beta-2 adrenoceptor have volumes of 11,469.52 Å<sup>3</sup> (red region in Figure 8.5), 5,143.08 Å<sup>3</sup> (purple region), 2,746.41 Å<sup>3</sup> (yellow region), and 1,429.31 Å<sup>3</sup> (red region).

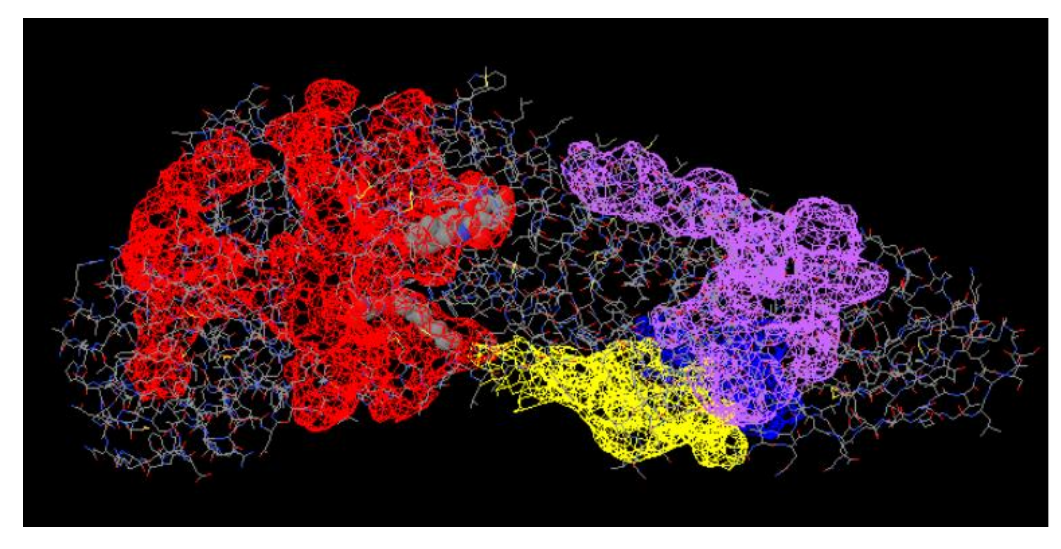


Figure 8.5: Main binding sites of the beta-2 adrenoceptor (4LDE) as generated by the PDBsum platform.

The four main binding pockets of the A2B adenosine receptor (8HDO), as shown in Figure 8.9, have volumes of 11,688.45 Å<sup>3</sup> (red), 11,017.69 Å<sup>3</sup> (violet), 2,959.45 Å<sup>3</sup> (yellow), and 2,381.91 Å<sup>3</sup> (red), respectively.

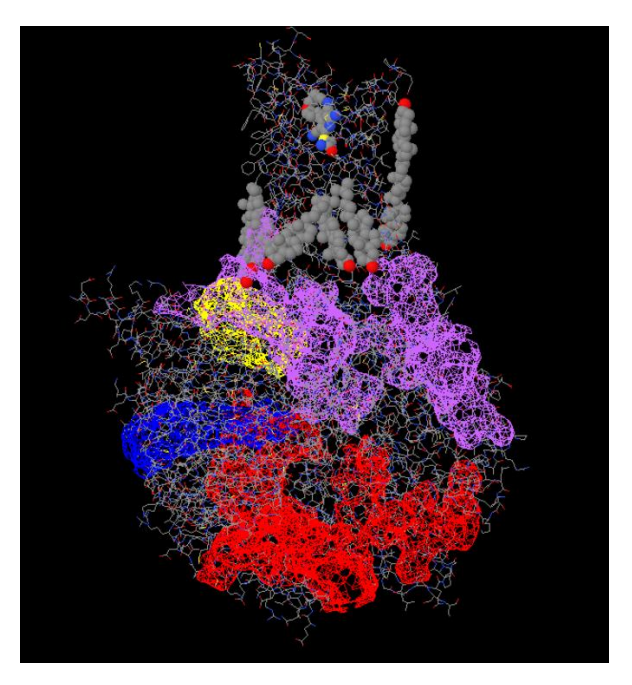


Figure 8.9: Secondary structures of the N and R chains of the A2B adenosine receptor (8HDO), as generated by the PDBsum platform.

The initial preparation for docking studies of these structures was carried out using the Python Molecular Viewer program (part of MGL Tools, version 1.5.7). The preparation steps included the removal of water molecules, any ligands and ions present in the X-ray structure, and the addition of hydrogen atoms, since these cannot be detected by X-rays.

#### 8.2 Preparation and characterization of ligand structures

The three-dimensional structures of the ligands (artemisinin, bilobalide, bilobetin, chelerythrine, chelidonine, epicatechin, gelsemic acid, ginkgolide A, isosilybin, silychristin, silybin, taraxacin, taraxacoside, taraxinic acid, rosmarinic acid, oleanolic acid, imatinib, sunitinib) were retrieved from the PubChem database. The following species were thus identified:

• Bilobetin: at the acidic pH of the stomach, the neutral form is predominant. As the pH increases, deprotonated species appear at the phenol-type hydroxyl groups (Figure 8.11).

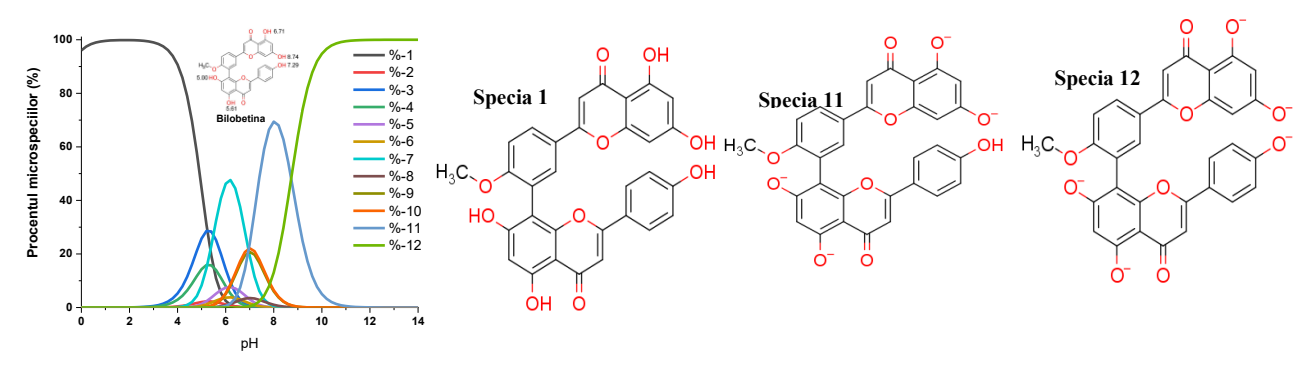


Figure 8.11: Possible microspecies present in solution for bilobetin depending on pH. Structures of the major species at pH 7.4 (species 11), very acidic pH (species 1), and very basic pH (species 12).

• Bilobalide exhibits only three species; up to pH 10, the neutral species is the only one present (Figure 8.12).

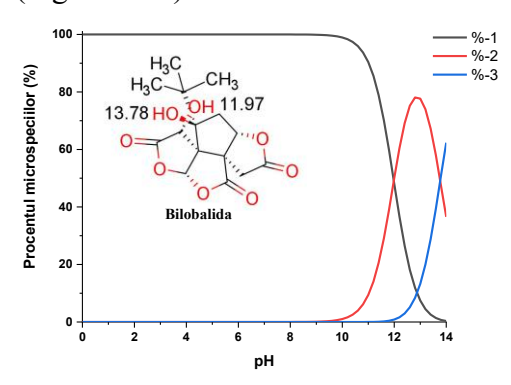


Figure 8.12: Possible microspecies of bilobalide present in solution as a function of pH. The predominant species at pH 7.4 and under strongly acidic conditions is species 1, while species 2 and 3 are predominant under highly basic conditions.

• Chelidonine (Figure 8.13) exists in its neutral form up to pH 4.5. As the pH increases, the nitrogen atom in the piperidine ring becomes protonated, making this the dominant species within the pH range of 6–14. Deprotonation of the hydroxyl group may also occur, but only under highly basic conditions, and the resulting species is present at low concentrations.

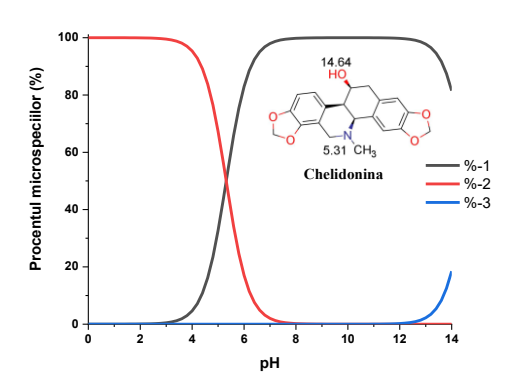


Figure 8.13 Predicted microspecies of chelidonine in aqueous solution as a function of pH. Major species at physiological pH 7.4 (species 1), under highly acidic conditions (species 2), and in strongly basic environments (species 3).

• Epicatechin is a polyphenol that exists exclusively in its neutral (non-ionized) form up to pH 8.5. At pH values between 8.5 and 12.5, several deprotonated forms may appear, whose composition is illustrated in Figure 8.14.

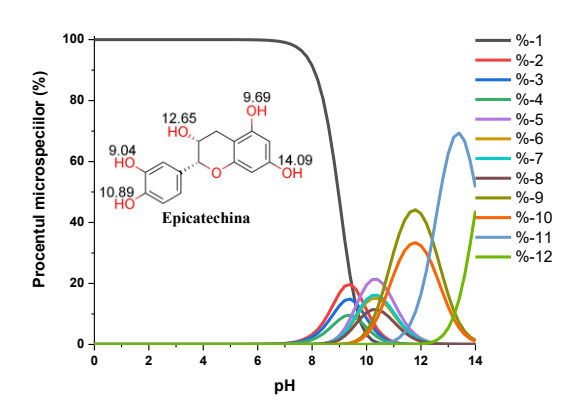


Figure 8.14: Possible microspecies of epicatechin present in solution as a function of pH. Structures of the major species at pH 7.4 (species 1), under highly acidic conditions (species 1), and under highly basic conditions (species 9 and 11).

• Gelseminic acid is a coumarin derivative that contains a phenolic group and, therefore, remains in its neutral form up to pH 6. Above this value, deprotonation of the phenolic hydroxyl group begins (Figure 8.15).

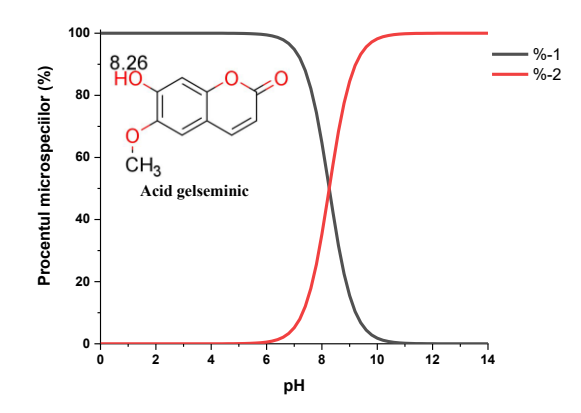


Figure 8.15: Possible microspecies of gelseminic acid in solution as a function of pH. The major species present at pH 7.4 (species 1), at very acidic pH (species 1), and at very basic pH (species 2).

• Ginkgolide A is a diterpene lactone whose neutral form predominates up to pH 10 (Figure 8.16).

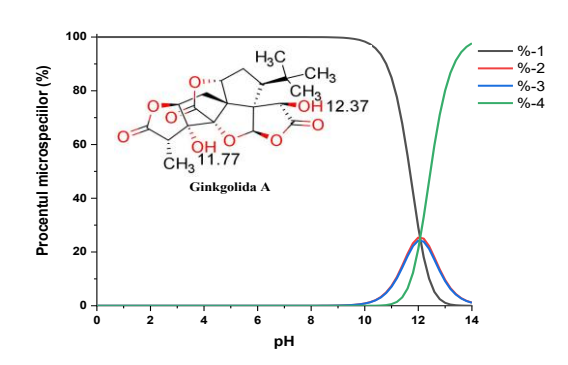


Figure 8.16: Possible microspecies of ginkgolide A present in solution depending on pH. Structures of the major species at pH 7.4 (species 1), strongly acidic pH (species 1), and highly basic pH (species 4).

• Isosilibinin (Figure 8.17) and silicristin (Figure 8.18), which possess hybrid structures combining flavonoid and lignan characteristics, remain in their non-protonated forms up to pH 6.

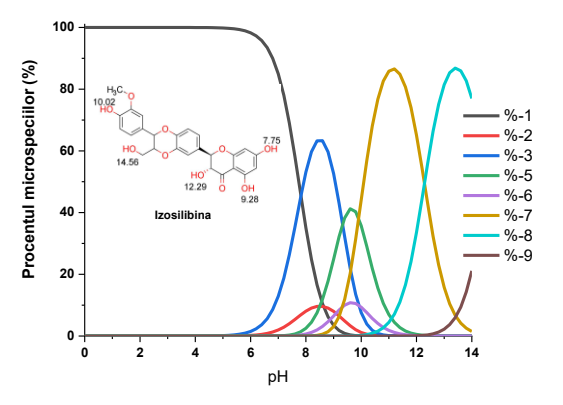


Figure 8.17: Possible microspecies present in solution for isosilibinin as a function of pH. Structures of the predominant species at pH 7.4 (species 1), under strongly acidic conditions (species 1), and under strongly basic conditions (species 7 and 8).

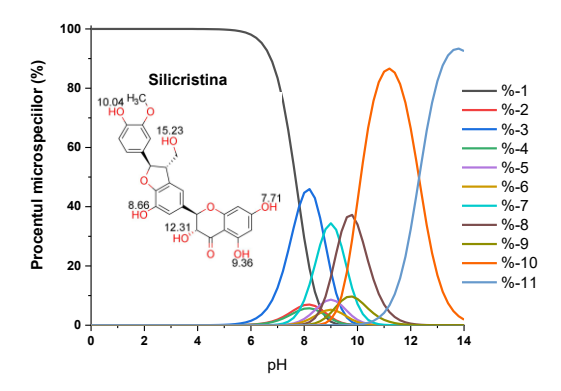


Figure 8.18: Possible microspecies present in solution for silychristin as a function of pH. Structures of the predominant species at pH 7.4 (species 1), under strongly acidic conditions (species 1), and under strongly basic conditions (species 10 and 11).

• Taraxacoside (Figure 8.19) is a glycoside acylated at a hydroxyl group. It contains a phenolic hydroxyl moiety that can undergo significant ionization at pH values above 9.

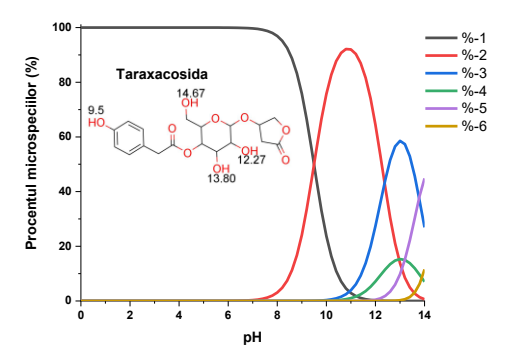


Figure 8.19: Possible microspecies of taraxacoside present in solution as a function of pH. The predominant structures correspond to species 1 at pH 7.4 and under highly acidic conditions, while species 3 and 5 are predominant under highly basic conditions.

• Taraxinic acid (Figure 8.20) contains a carboxyl group that can undergo ionization, with the resulting species being predominant in the pH range of 6–14.

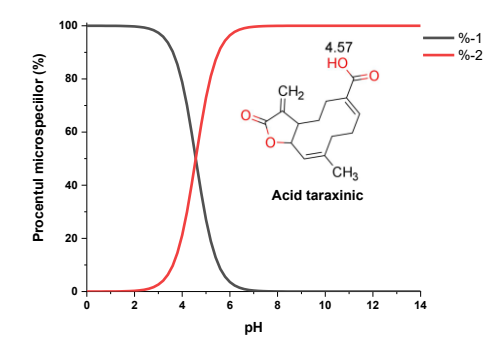


Figure 8.20: Possible microspecies of taraxinic acid present in solution depending on pH. The major species at pH 7.4 is species 2, at very acidic pH is species 1, and at very basic pH is also species 2.

• At acidic pH, sunitinib is protonated at the tertiary amino group (Figure 8.21), while imatinib can undergo protonation at multiple amine functional groups (Figure 8.22).

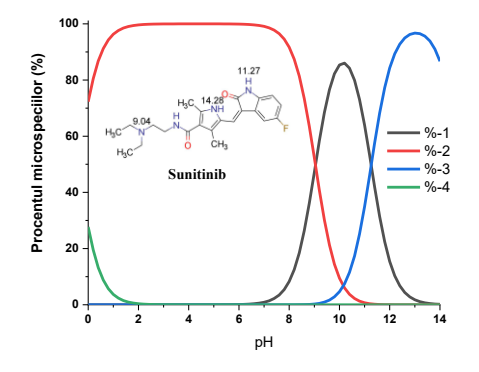


Figure 8.21: Possible microspecies of sunitinib present in solution as a function of pH. Structures of the major species at pH 7.4 (species 1), strongly acidic pH (species 2), and strongly basic pH (species 3).

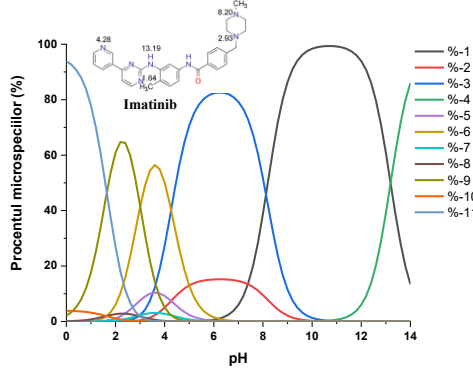


Figure 8.22: Possible microspecies of imatinib present in solution as a function of pH. Structures of the major species at pH 7.4 (species 3), strongly acidic pH (species 11), and strongly basic pH (species 1).

Prior to the docking studies, the ligand molecules were processed (protonated/deprotonated) based on the predominant microspecies at the considered pH, and their structures were optimized to reach a geometry corresponding to a local energy minimum. Geometry optimization was performed using the Open Babel platform, version 3.0 [252]. In addition, Gasteiger partial atomic charges were computed.

Rosmarinic acid from Melissa officinalis binds with lower affinity to the imatinib and sunitinib binding site (-7.89 kcal/mol) on the A2B adenosine receptor corresponding to chain R. However, it exhibits a higher affinity for chain B (-9.70 kcal/mol). Therefore, in the presence of sunitinib and imatinib, the binding affinity remains high (-9.68 kcal/mol and -9.52 kcal/mol, respectively) (Figure 8.26).

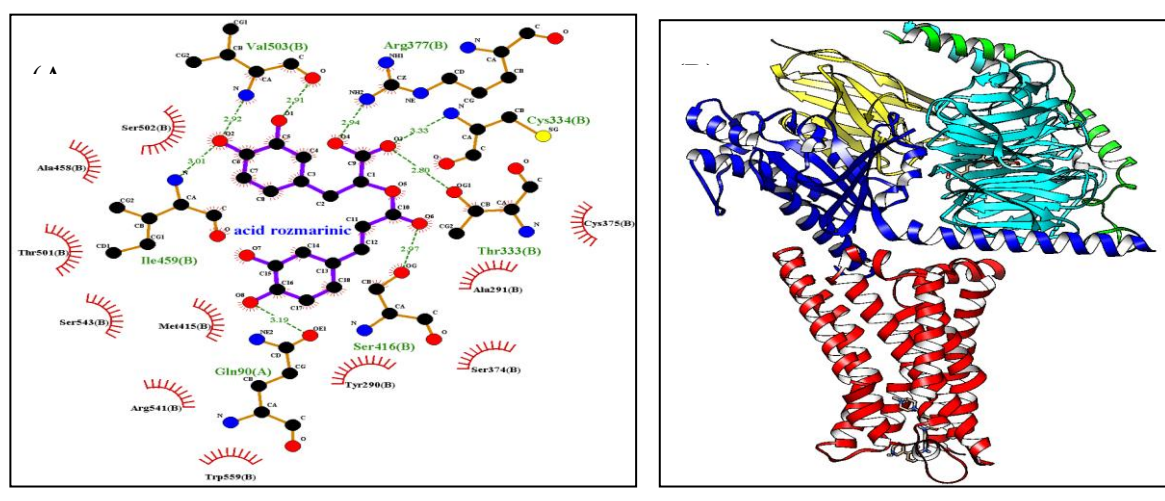


Figure 8.26: (A) Main types of interactions between rosmarinic acid from Melissa officinalis and the amino acid residues within the A2B adenosine receptor. (B) Structure of the rosmarinic acid—A2B adenosine receptor complex in the presence of imatinib (bound to chain R, highlighted in red in the structure).

Silibinin from *Silybum marianum* binds to the same binding site on the apelin receptor as imatinib and sunitinib. On its own, it exhibits a strong binding affinity (-9.40 kcal/mol), greater than that of sunitinib (-8.14 kcal/mol), but slightly lower than that of imatinib (-9.66 kcal/mol). However, in the presence of either drug, competition for the binding site leads to a significant decrease in affinity:

- -7.89 kcal/mol in the presence of sunitinib
- -7.67 kcal/mol in the presence of imatinib (Figure 8.27).

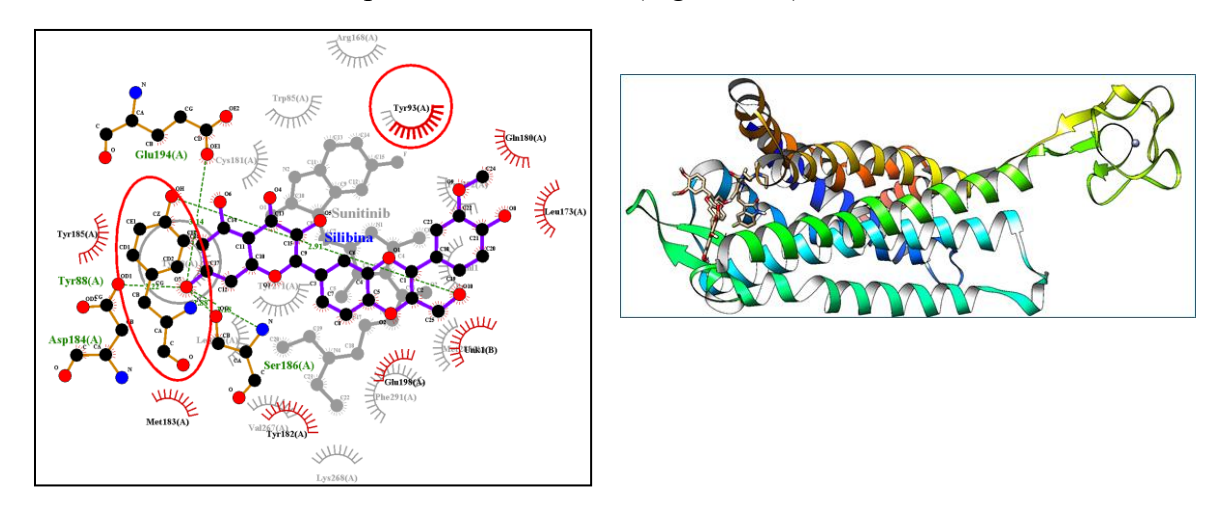
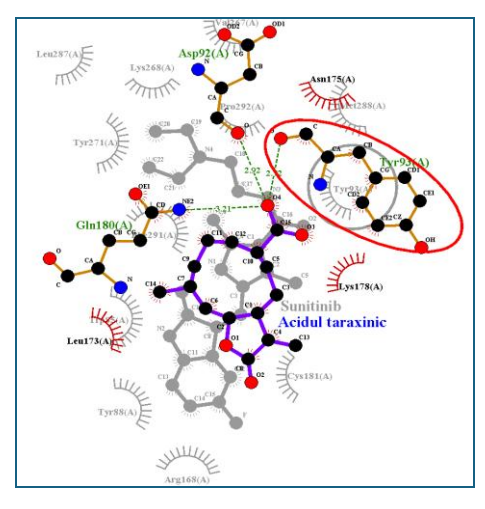


Figure 8.27: (A) Main types of interactions between silibinin from Silybum marianum and the amino acid residues of the apelin receptor in the presence of sunitinib. (B) Structure of the silibinin–apelin receptor complex in the presence of sunitinib.

Taraxinic acid from *Silybum marianum* and *Taraxacum officinale* exhibits relatively low affinity for all three studied receptors (Table VIII.I). In the case of the apelin receptor, it binds to the same site as sunitinib (Figure 8.28) and imatinib, which further decreases its affinity when binding occurs in their presence (from -8.60 kcal/mol to -6.20 kcal/mol and -5.69 kcal/mol, respectively).



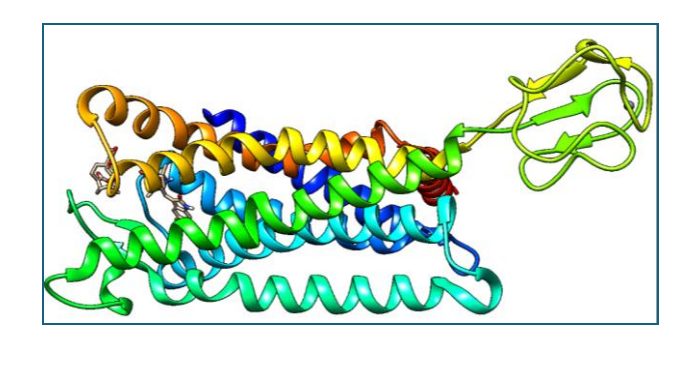
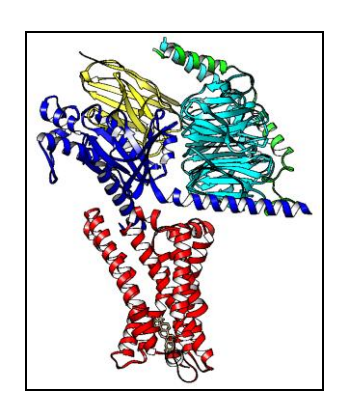
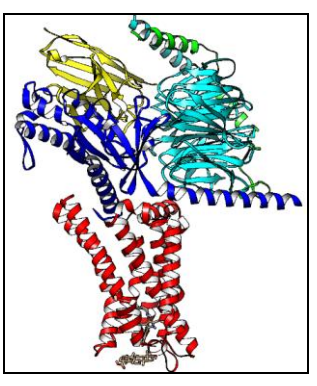
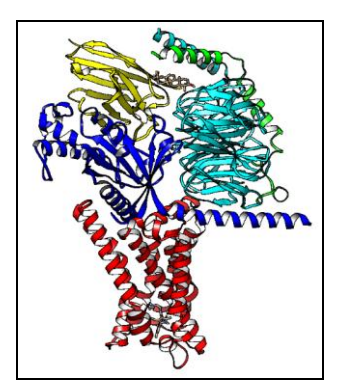


Figure 8.28: (A) Main types of interactions between taraxinic acid from Silybum marianum and Taraxacum officinale and the amino acid residues of the apelin receptor in the presence of sunitinib. (B) Structure of the taraxinic acid—apelin receptor complex in the presence of sunitinib.

Oleanolic acid from *Clematis vitalba* exhibits high affinity for the A2B adenosine receptor (–9.76 kcal/mol) and the apelin receptor (–8.57 kcal/mol), while showing lower reactivity toward the β2-adrenergic receptor (–7.43 kcal/mol) (Table VIII.1). In the presence of sunitinib, binding to the same site on the A2B adenosine receptor is significantly affected, with the affinity dropping to –5.34 kcal/mol (Figure 8.29).







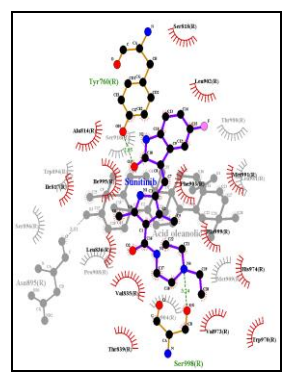


Figure 8.29: Structure of the oleanolic acid—A2B adenosine receptor complex: (A) binding of oleanolic acid from Clematis vitalba to the receptor; (B) co-binding with sunitinib at the same binding site; (C) simultaneous binding at distinct sites on the receptor; (D) main types of interactions between oleanolic acid and the amino acid residues of the A2B adenosine receptor.

Based on the molecular docking simulations, many of the studied compounds exhibited high predicted binding affinities toward the analyzed receptors. These findings highlight their potential as candidate molecules for experimental validation and further investigation as modulators of receptor interactions in cancer cell lines.

# CHAPTER IX: EVALUATION OF ADVERSE EFFECTS AND SAFETY OF ONCOTHERAPIES

# ASSESSMENT OF ADVERSE EFFECTS AND SAFETY OF ONCOLOGICAL TREATMENTS

#### 9.1 Introduction

Recording adverse events plays a crucial role in the accumulation of essential data necessary for evaluating the safety of drug therapies. Reporting such reactions leads to improvements in the quality and efficacy of available treatments.

Cisplatin, a platinum-based chemotherapeutic agent, is widely used in the treatment of testicular, ovarian, lung, bladder, and other solid tumors. Despite its effectiveness, it is well known for its severe toxicities, including nephrotoxicity, ototoxicity, peripheral neuropathy, severe nausea and vomiting, myelosuppression, and vascular toxicity.

Imatinib and sunitinib, both tyrosine kinase inhibitors, represent significant advances in cancer therapy. However, their use is limited by specific toxicities that may affect treatment adherence and patients' quality of life.

The objective of this study is to analyze adverse reactions reported for imatinib, sunitinib, and cisplatin in the EudraVigilance database, in order to compare the safety profiles of these antineoplastic agents, which have distinct mechanisms of action but overlapping indications in oncology.

### 9.2. Pharmacovigilance of Cisplatin

The number of Individual Case Safety Reports (ICSRs) identified in the EudraVigilance database for Cisplatin amounts to 36,347 as of February 9, 2025.

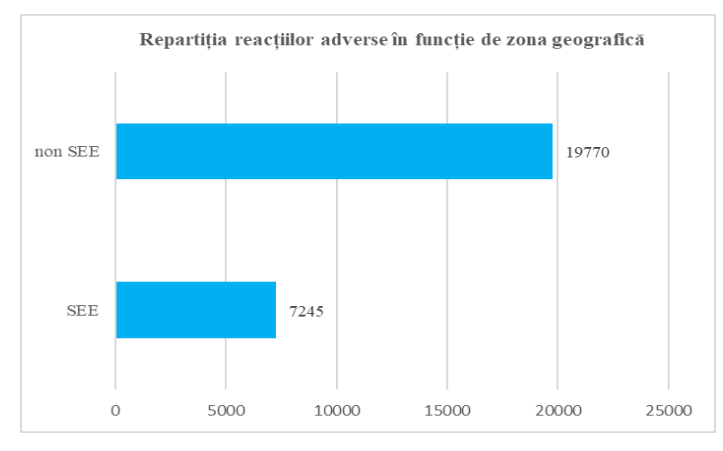


Figure 9.1: The number of adverse reaction cases by geographical region.

Of the total cases, 37.3% originated from countries within the European Economic Area (EEA), while 62.7% were reported from non-EEA countries.

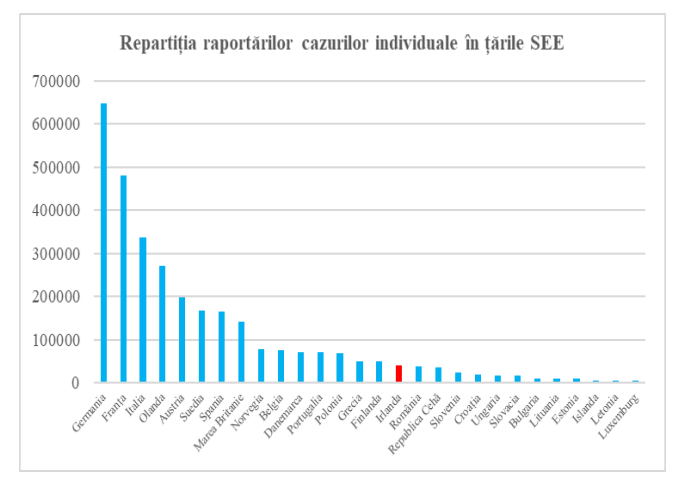
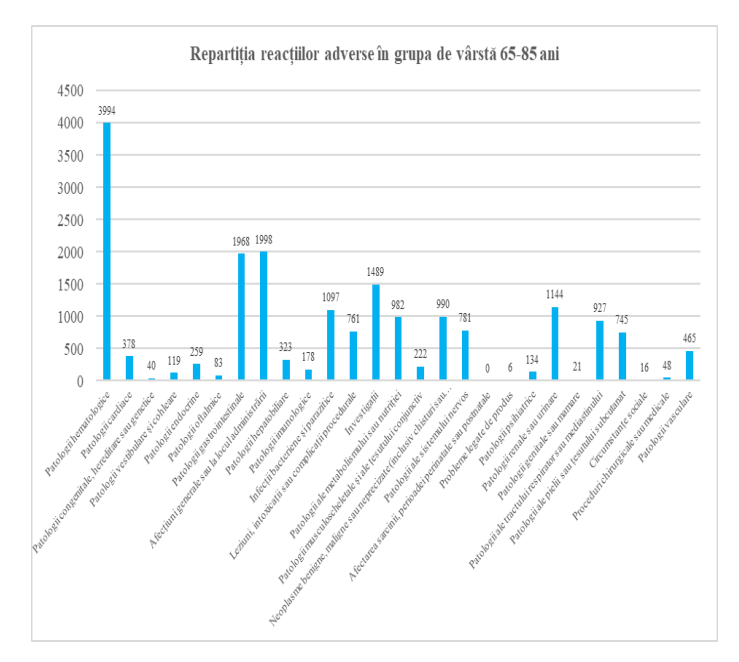


Figure 9.2: Number of individual cases reported in EEA countries

The highest reporting rates were recorded in Italy (3,270 reports), France (3,031 cases), Poland (1,750 cases), and Germany (1,272 cases), while Romania ranked 16th with 125 reports (0.92%).



In the 65–85 age group, the most frequently reported adverse reactions are associated with hematological disorders (20.84%), general disorders or administration site conditions (10.42%), and gastrointestinal disorders (10.42%).

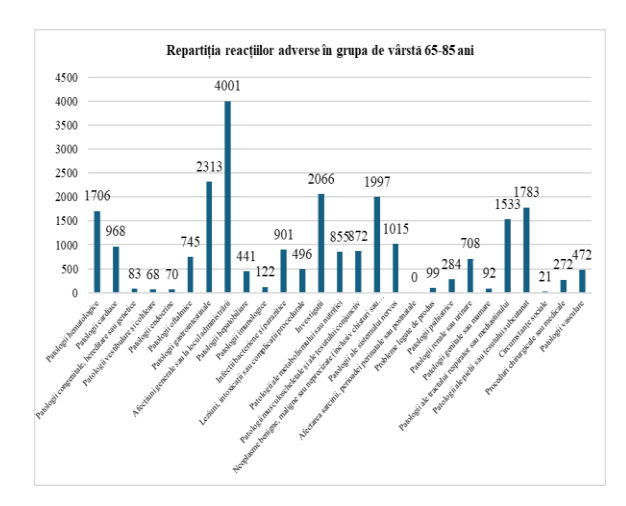
Figure 9.10: Number of adverse reaction cases in the 65-85 age group, by type of reaction

Serious adverse reactions predominate in most reaction categories, particularly in blood and lymphatic disorders, gastrointestinal, and cardiovascular conditions, being closely associated with cisplatin-induced bone marrow toxicity.

### 9.3 Pharmacovigilance of Tyrosine Kinase Inhibitors

#### 9.3.1. Imatinib

The number of individual cases identified in the EudraVigilance database for IMATINIB is 46,255, as of February 9, 2025.



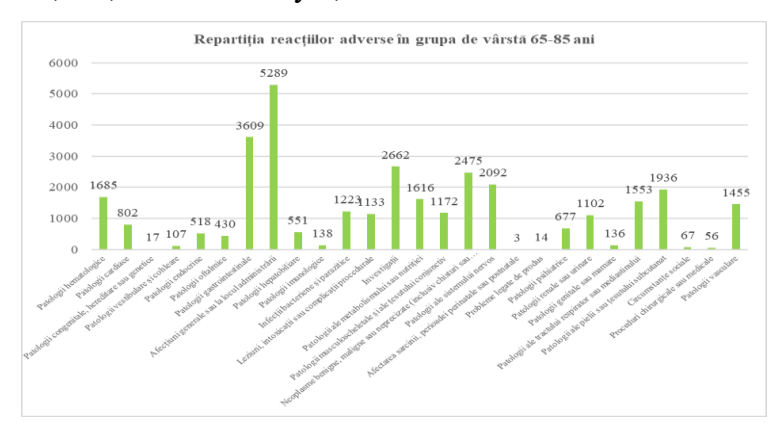
In the 65–85 age group, the most frequently reported adverse reactions are related to general disorders and administration site conditions (16.68%), gastrointestinal disorders (9.64%), and benign, malignant, or unspecified neoplasms — including cysts and polyps (8.33%).

Figure 9.20: Number of adverse reaction cases in the 65–85 age group, by type of reaction

Almost all reported adverse reactions are classified as serious (92.12%). This is a major concern, given that imatinib is used in oncologic treatments where the risks may be higher due to the nature of the disease and the side effects. Continuous monitoring and dose adjustment are essential to mitigate these risks.

#### 9.3.2. Sunitinib

The total number of individual cases identified in Eudra Vigilance for SUNITINIB is 27,015, as of February 9, 2025.



The most frequently reported adverse reactions are those related to general disorders and administration site conditions (6.98%), followed by gastrointestinal disorders (4.76%).

Figure 9.30: Number of adverse reaction cases in the 65–85 age group, by type of reaction

The most frequently reported adverse reactions included general disorders and administration site conditions, gastrointestinal disorders, neoplasms, nervous system disorders, and subcutaneous tissue disorders. Data on sunitinib indicate a higher prevalence of adverse reactions among male patients and those in adult age groups, with serious cases accounting for the majority of reports.

#### 9.4. Conclusions

Thus, each of the three drugs exhibits a distinct adverse reaction profile, with notable overlaps in terms of general, gastrointestinal, and hematological effects, as well as specific features that reflect their differing pharmacological mechanisms and the particular patient populations for which they are intended.

### CHAPTER X: CASE STUDY: PHGIST: PRIMARY HEPATIC GASTRO-INTESTINAL STROMAL TUMOR

#### 10.1 Introduction

Gastrointestinal stromal tumors (GISTs) represent the most common form of mesenchymal tumors of the digestive tract, originating from the interstitial cells of Cajal. Typically, these tumors occur in extrahepatic locations; however, a small percentage arise in the liver and are termed primary hepatic gastrointestinal stromal tumors (PHGIST). The diagnosis of PHGIST is made by exclusion, as they share the same immunohistochemical and histological molecular characteristics as classical gastrointestinal stromal tumors. Due to the limited number of published studies, data regarding morbidity and mortality associated with PHGIST remain scarce. Immunohistopathology may aid in developing screening recommendations and in assessing treatment resistance [77].

To illustrate this particular clinical scenario, we present the case of patient S.D.M., a 79-year-old female with no personal pathological history or chronic treatments.

#### 10.2 Clinical Case Stages

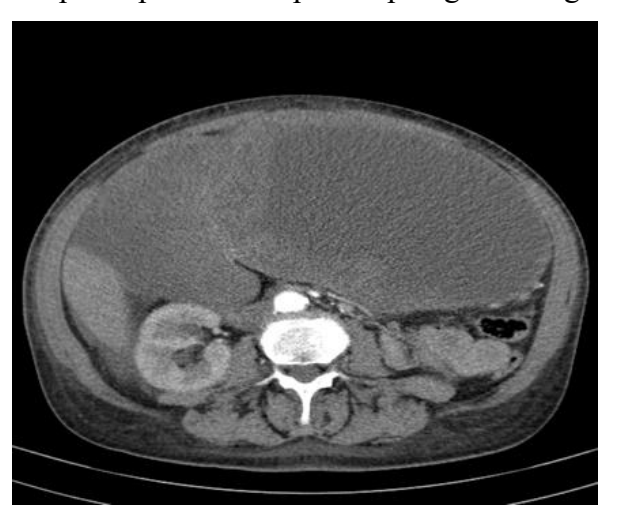
#### Stage 0: Prediagnostic Period: 22.02.2017 to 27.02.2017

The patient presented with marked fatigue, anorexia, moderate weight loss, and abdominal distension. Clinical examination revealed a pale-appearing patient exhibiting signs of asthenia, with a mildly compromised general condition. The abdomen was markedly distended and symmetric, with a large volume of tense ascites; intestinal transit was normal, and respiratory dysfunction of a restrictive pattern was noted. Additionally, the digital rectal examination was within normal limits.



Figure 10.1: CT Appearance at Diagnosis – Hepatic tumor formations exhibiting a cystic appearance, with walls of variable thickness and heterogeneous contrast enhancement.

On transverse sections, three parenchymal calcifications are evident in the right hepatic lobe: the largest measures 14 mm, the smallest between 2 and 3 mm, with two of them in contact with the cystic wall. Within segments IVB and III, two large masses occupy nearly the entire peritoneal cavity. The gallbladder is not identifiable, most likely compressed by the adjacent mass. Additionally, a variable-thickness fluid layer measuring between 1 and 3 cm is observed in the perihepatic and hepatodiaphragmatic regions.



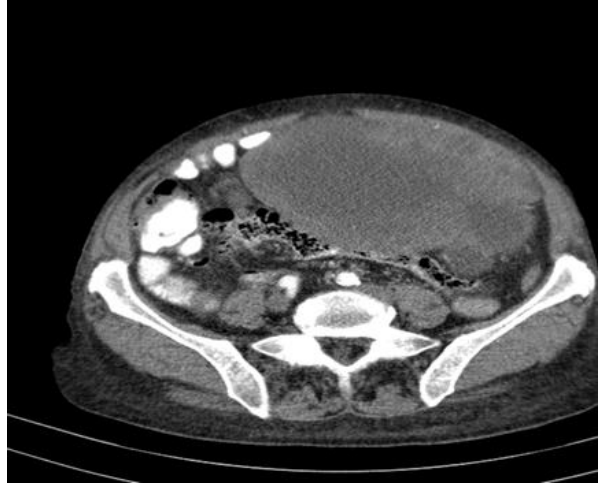


Figure 10.2: CT Appearance at Diagnosis – The inferior pole of the cystic mass in the left hepatic lobe extends into the pelvis (measuring 14 x 18 x 18.5 cm) and displaces the transverse colon and small intestine posteriorly toward the right iliac fossa.

After correcting the hydroelectrolytic imbalance and anemia, surgical intervention was planned with the aim of confirming the diagnosis and performing a debulking tumorectomy.

#### Stage I: First surgical intervention: 01.03.2017 to 01.04.2017

Hospital Admission — CF1 Witting Hospital, Bucharest: Surgical clinical examination upon admission revealed a markedly enlarged, tense abdomen with significant hepatomegaly involving both lobes. The inferior margin of the left lobe extended down to the left iliac fossa.



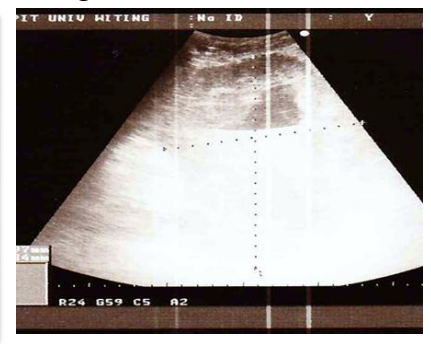




Figura 10.3: Aspecte ecografice în momentul diagnosticării

Surgical intervention was performed due to a giant polycystic hepatic tumor mass that practically replaced both hepatic lobes, characterized by large cystic cavities containing clear fluid. The cystic formation in the left lobe extended down to the left iliac fossa. The tumor exhibited an encephaloid appearance, was slightly friable, bled profusely, adhered to the

intestinal mass, and could not be mobilized. Moderate ascitic fluid was present. The hepatic parenchyma appeared normal only in segments VI-VII.

The procedure included diagnostic laparotomy, excisional biopsy, evacuation of the cystic tumor formation in the left hepatic lobe, intracavitary drainage, and multiple peritoneal drainages. Biopsy specimens (fragments measuring 1–3.5 cm) were sent for anatomopathological examination, which revealed tumor proliferation composed of clear mesenchymal-origin cells, confirming GIST by immunohistochemical analysis.

The postoperative course was initially prolonged, with significant hemorrhagic ascitic fluid loss through peritoneal drains, necessitating repeated red blood cell transfusions. The patient was discharged 30 days after admission, with a healed surgical site, active intestinal transit, and oral intake, although a peritoneal drainage of approximately 500 ml/day with ascitic appearance persisted.

Anatomopathological examination showed tumor tissue fragments composed of spindle cells with clear vacuolar cytoplasm and relatively homogeneous oval nuclei exhibiting tachychromasia and vacuolization; nucleoli were difficult to discern. Cellular borders were indistinct, and cells arranged around ectatic thin-walled vessels. Mitotic activity was low (3 mitoses per 50 high-power fields). Histopathological analysis concluded the tumor was a clear cell mesenteric-origin proliferation consistent with GIST.

To establish a definitive diagnosis, tumor fragments underwent immunohistochemistry using an extensive panel of immunomarkers with the following results:

- CD117, VIMENTIN, PDGFR-Alpha, CD34, DOG1 were positive in tumor cells;
- ACTININ was negative in tumor cells but positive in vessels;
- Ki67 was positive with a proliferation index of 25% in tumor cells;
- S100 was negative.

The immunohistochemical findings led to the diagnosis of a malignant primary hepatic gastrointestinal stromal tumor (GIST).

### Stage II: First-Line Tyrosine Kinase Inhibitor Treatment – IMATINIB: 03.05.2017 to 05.05.2021

Treatment with IMATINIB (GLIVEC) 400 mg, administered as 2 tablets per day, was initiated, leading to a rapid improvement in the patient's general condition, a reduction in drainage to 50 ml/24h, decreased abdominal volume, and removal of drainage tubes approximately one month after therapy initiation.

At 6 months, imaging follow-up demonstrated a partial response to tyrosine kinase inhibitor therapy according to the Choi criteria, characterized by a reduction in the size and density of the hepatic tumor formations.

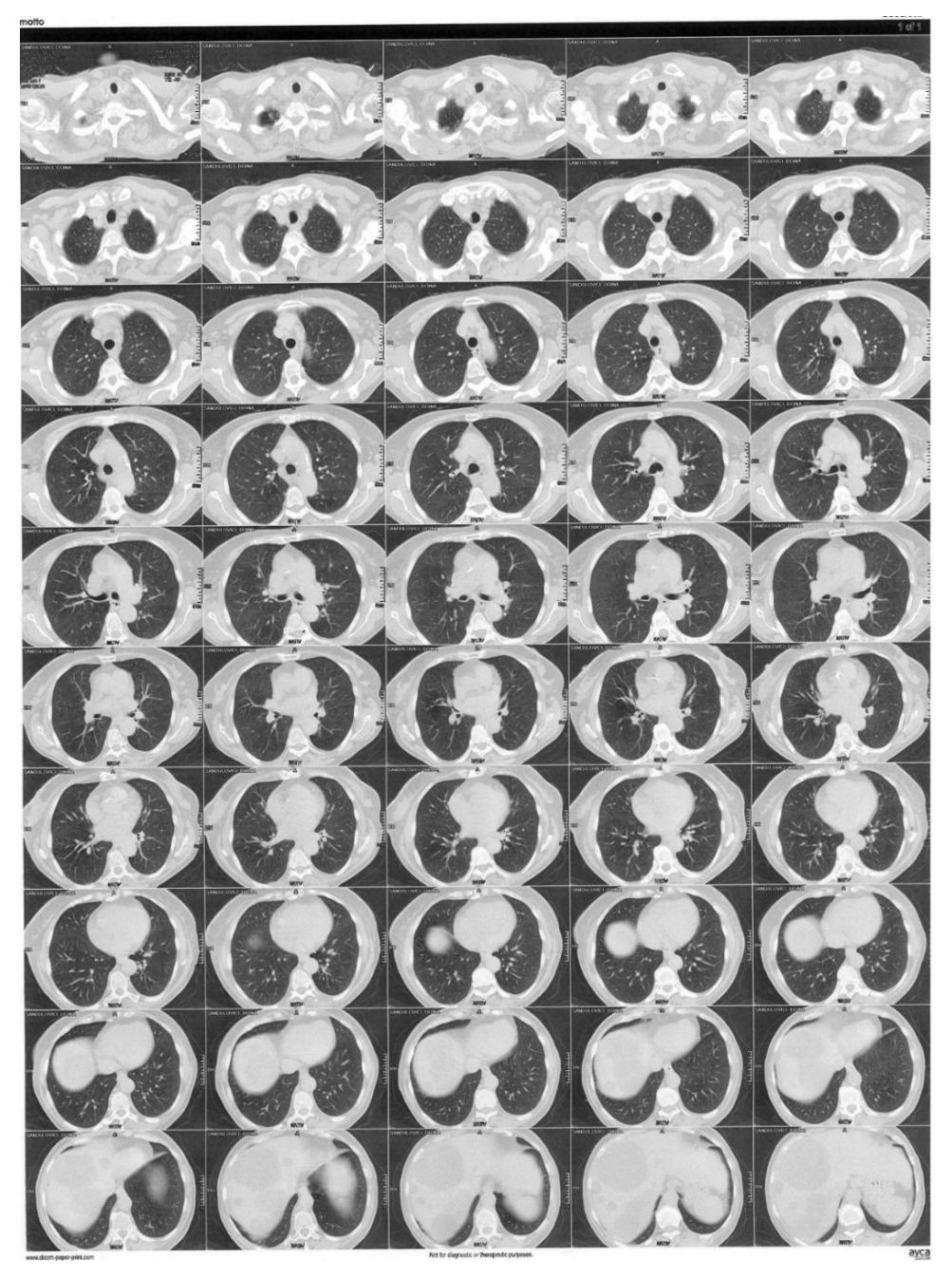


Figure 10.4.1: CT Appearance at 6 Months

The largest intrahepatic tumor measures 90 x 54 x 46 mm, located between segments II and III. The hepatic tumor formations demonstrate less intense contrast enhancement compared to the previous evaluation.

As of 03.03.2021, four years after diagnosis, the liver exhibits multiple simple biliary macro-cysts up to 8 cm in size, previously described and stable over time. The gallbladder appears free of calculi. A nonspecific stationary nodule measuring 35 x 22 mm is present in Morrison's pouch. The kidneys are functional, without tumors, hydronephrosis, or calculi. No suspicious adrenal nodules are noted. The pancreas appears homogeneous.

The stomach shows parietal changes at the antral level over approximately 4 cm, with circumferential wall thickening up to 14 mm. No celiac, mesenteric, or retroperitoneal

lymphadenopathy with macroscopic tumor features is observed. The urinary bladder is evacuated. Moderate diffuse fecal stasis is present. No ascites detected. The uterus is small and involuted. The adnexal regions are free. The axial skeleton included in the imaging shows no secondary lesions.

#### Stage III: Onset of Resistance to IMATINIB: 14.06.2021 to 03.12.2021

Multiple cystic hepatic tumors measuring up to 8 cm in the right lobe, stable compared to previous investigations. A subcapsular mass with extrahepatic extension in Morrison's pouch, isodense with hepatic parenchyma, measuring 3 x 3.7 cm, also stationary.



Figure: 10.10.1: CT Appearance at 48 Months Under Imatinib Treatment

The gallbladder is distended, with common bile duct (CBD) and intrahepatic bile ducts (IHBD) not dilated. The pancreas appears homogeneous. The stomach shows hypertrophic folds. The gastric antrum walls exhibit segmental variable thickness: 14 mm proximally and 8 mm more distally - findings stable compared to March 2021.

#### Stage IV: Discontinuation of IMATINIB Treatment: 04.01.2022 to 26.06.2022

A newly appeared large cystic tumor mass measuring 12 x 12 cm is noted in the epigastric region, likely originating from the posterior wall of the gastric antrum, impressing upon the inferior margin of the left hepatic lobe. The rest of the findings remain stable.

The cystic tumor formation has an iodophilic wall with a centrally parafluid density. The mass is contiguous with the inferior left margin of the liver and the posterior wall of the gastric antrum, measuring 12 x 12 cm.

Based on these findings, discontinuation of first-line tyrosine kinase inhibitor therapy — Imatinib - was decided.

#### Stage V: Second surgical intervention: 27.06.2022 to 11.07.2022

The patient was admitted to presenting with sporadic, low-volume vomiting, physical asthenia, and a large, palpable tumor mass in the epigastric region, described as hard, immobile,

and non-tender. Clinical and paraclinical investigations (EKG, chest X-ray, upper digestive endoscopy) revealed no other pathological changes; the stomach was posteriorly impressed in the vertical region without mucosal lesions. Laboratory tests showed chronic normochromic, normocytic anemia with hemoglobin at 8.4 g/dl.

Surgical intervention was performed for a cystic tumor formation of the left hepatic lobe - detached from the left hepatic lobe, extending posteriorly to the plane of the major vessels, inferiorly to the transverse mesocolon, measuring approximately 12 x 15 cm, tense with a relatively fibrous wall.

The patient was transferred to the Fundeni Clinical Institute, General Surgery Clinic. A reoperation was performed on 04.07.2022 with the diagnosis of a large cystic tumor in segment III. An atypical segment III hepatectomy en bloc with the tumor formation was performed.

Postoperatively, the patient's evolution was favorable, afebrile, with resumption of intestinal transit for gas and feces, and decreased output from the peritoneal drainage tubes, which were removed after a control ultrasound described: residual liver with heterogeneous echotexture due to several macronodular lesions with transonic content in segments VII-VIII and other nodular lesions with heterogeneous structure in segments VI-VII; patent hepatic vascular axes; no dilation of the biliary tree; spleen and kidneys without abnormalities; no ascites or intraabdominal collections.

The patient was discharged in good general condition, with digestive tolerance and a surgically healing wound. General postoperative recommendations were provided.

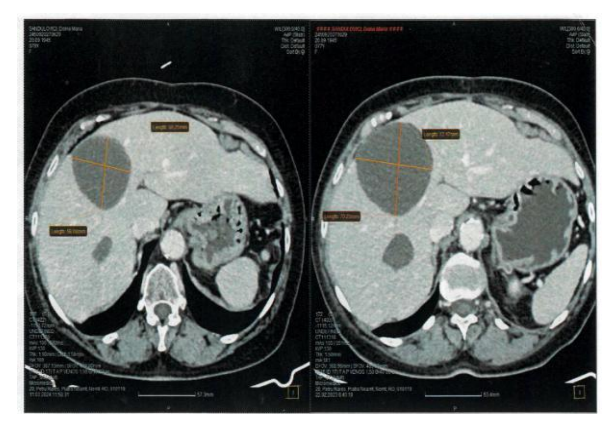
### Stage VI: Second-Line Tyrosine Kinase Inhibitor Treatment – SUNITINIB: 04.11.2022 to 23.01.2025

One month postoperatively, second-line treatment with Sunitinib was initiated. A cardiological evaluation including ejection fraction (EF) was required. The cardiology consultation revealed mild degenerative valvopathies and mild dyslipidemia, with no contraindications for oncological treatment.

The histopathological (HP) aspect was suggestive of mesenchymal tumors with spindle cells (GIST type). Immunohistochemical (IHC) tests supported the diagnosis of a high-grade malignant gastrointestinal stromal tumor (secondary determination). The second-line treatment with Sunitinib started at 50 mg/day for 28 days followed by a 14-day break.

At the CT scan performed after 15 months of Sunitinib treatment, the known hepatic lesions remained stable. No new suspicious lesions suggestive of metastases were detected in the thoraco-abdomin-pelvic region compared to the previous examination before Sunitinib initiation.

At six and a half years post-diagnosis and 18 years after the last CT scan, a new cystic hepatic lesion appeared in segment VII. Most known cystic hepatic lesions had decreased in size. The previously seen tissue lesion in segment VI was no longer visualized. No new secondary lesions were identified in the lungs or bones. Significant stenoses were noted in the superficial femoral arteries.



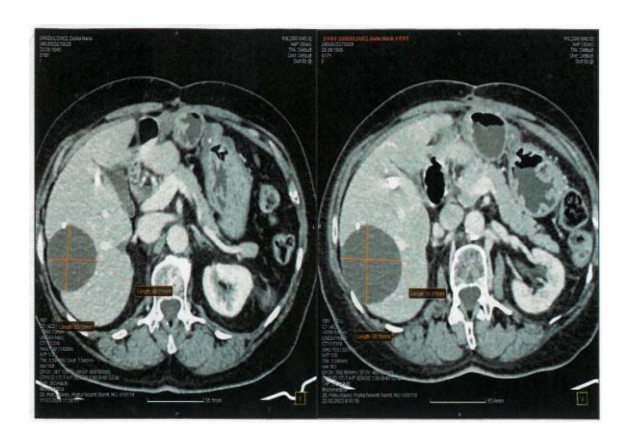


Figure 10.11.2: CT appearance at 18 months under Sunitinib Figure 10.11.3: CT appearance at 18 months under Sunitinib treatment

treatment

The appearance of a 21 x 24 mm subcapsular cystic lesion in segment VII.

#### 10.3 Clinical particularities of the case

A noteworthy aspect is that despite the use of advanced imaging techniques and exploratory laparotomy, the origin of the GIST in the gastrointestinal tract (GIT) was not identified. Although immunohistochemical examination suggests a possible hepatic origin, some authors challenge this conclusion, arguing that tumors arising in parenchymal organs (liver, pancreas, prostate) may represent metastases resulting from direct extension of GISTs originating from hollow digestive organs.

This case presents several atypical and complex features that distinguish it from other cases of primary hepatic GIST (PHGIST): a prolonged disease course with long-term treatment, a predominantly cystic tumor mass of considerable size, resistance to Imatinib, and severe adverse effects from tyrosine kinase inhibitor (TKI) therapies.

The literature indicates that PHGIST is a rare and challenging pathology with a guarded prognosis. Nevertheless, the patient achieved an 8-year survival from diagnosis, which is remarkable. Reported cases in the literature note median survival rates are significantly shorter, with 5-year survival around 33% in some studies [77].

In the majority of PHGIST cases, tumors are solid and may present central necrosis; however, cystic cases are rare. In this patient, the hepatic tumors exhibited predominantly cystic behavior with unusually large dimensions, reaching up to 12 x 12 cm.

After approximately four years of treatment, the patient developed resistance to first-line tyrosine kinase inhibitors (TKIs), a phenomenon reported in the literature but typically observed earlier (after 2–3 years).

The severe adverse effects reported by the patient during TKI therapy included:

Imatinib: intense muscle spasms throughout the treatment period,

- Sunitinib: moderate to severe hypertension, nail bed keratinization, alopecia, bilateral cataract development, and severe anemia managed with supplemental iron.

These adverse effects, particularly those associated with Sunitinib, are less frequently reported but fall within the spectrum of cutaneous and vascular toxicities described in the literature.

Unique features of the case include:

- Prolonged survival (>7 years) despite a pathology with a generally poor prognosis,
- The cystic nature of the tumor, which is rarely encountered in PHGIST,
- Severe side effects from TKI therapies, especially keratinization disorders, bilateral cataracts, and progressive peripheral and central arterial stenosis,
- Complex surgical interventions are complicated by severe postoperative complications.

#### 10.6 Conclusions

The presented case illustrates the complexity of diagnosing, treating, and monitoring the progression of Primary Hepatic Gastrointestinal Stromal Tumor (PHGIST), a rare and controversial entity in the specialized literature. The biochemical and clinical particularities revealed a complex interplay between the tumor process, systemic treatments with tyrosine kinase inhibitors (TKIs), and the biological response of the organism.

From a hematological and biochemical standpoint, the patient exhibited an overall stable profile, significantly influenced by treatment with Imatinib and Sunitinib. Persistent anemia syndrome, immunological changes suggestive of chronic tumor-related inflammation, and hematological and metabolic adverse effects—such as transient leukopenia requiring careful monitoring and therapeutic adjustment—were noted.

Clinically, the disease course was marked by an atypical presentation, including large cystic hepatic tumors, diagnostic challenges due to the absence of an evident primary digestive lesion, development of resistance to Imatinib after a longer period than typically reported in the literature, and rare but severe adverse effects associated with TKI therapy, such as bilateral cataracts, keratinization disorders, and progressive vascular stenoses.

The multimodal treatment approach, consisting of sequential administration of TKIs and major surgical interventions, enabled a remarkable survival exceeding eight years, despite the generally poor prognosis characteristic of this tumor type. This underscores the importance of rigorous monitoring, individualized therapeutic adaptation, and multidisciplinary collaboration in managing rare oncological cases.

Furthermore, this case raises questions about the validity of diagnosing PHGIST as a primary entity, since the hepatic origin of the tumor remains a subject of debate. Nevertheless, clinico-pathological and evolutionary data support the uniqueness of this case and highlight the need to reconsider diagnostic criteria in the context of atypical GIST presentations.

•

#### GENERAL CONCLUSIONS

### 1. Nanoparticles and plant extracts represent a promising direction in oncological therapies.

The results indicate that biosynthesized silver nanoparticles derived from plant extracts may play a significant role in anticancer treatments. These nanoparticles provide moderate cytotoxicity—less aggressive than cisplatin but more effective than simple plant extracts. The synergy between nanoparticles and plant extracts enhances treatment efficacy, reduces adverse effects, and protects healthy cells. Moreover, such combinations may decrease the toxicity of conventional therapies, improving their long-term tolerability.

### 2. Plant extracts have significant therapeutic potential but require standardization and thorough investigation.

Bioactive compounds extracted from plants such as greater celandine, dandelion, and lemon balm have demonstrated antitumor, antioxidant, and antimicrobial effects. They can modulate cellular responses to conventional treatments, offering a safer alternative or an adjuvant to increase chemotherapy efficacy. However, observed variability between different extracts and extraction methods underscores the need for further studies to standardize dosages and elucidate precise mechanisms of action.

### 3. Synergism between conventional and alternative therapies may optimize cancer treatments.

Data suggest that combined administration of oncological drugs with plant extracts or nanoparticles can improve the viability reduction of cancer cells, enhancing treatment effectiveness. Some combinations also showed protective effects on normal cells, potentially reducing chemotherapy side effects. These findings highlight the importance of combinational therapeutic strategies that allow lower chemotherapeutic dosages while maintaining treatment efficacy.

# 4. The antioxidant and antimicrobial activities of plant extracts suggest broad applications in preventive medicine.

Polyphenol-rich plants like Melissa officinalis and Clematis vitalba demonstrated strong antioxidant effects, potentially contributing to the prevention of oxidative stress-related diseases including cancer and neurodegenerative disorders. Additionally, antimicrobial activities observed suggest potential use against bacterial and fungal infections. These findings open avenues for developing natural therapies against antibiotic-resistant infections and chronic diseases linked to oxidative stress.

# 5. The adverse reaction profiles of current chemotherapeutics necessitate careful monitoring and personalized treatment.

Pharmacovigilance analyses revealed that widely used oncological drugs such as cisplatin, imatinib, and sunitinib have significant toxicity profiles, especially in elderly patients and males. Common adverse effects include gastrointestinal, hematological, and renal disorders, with most reports indicating severe outcomes. This underscores the need for continuous patient monitoring and treatment adjustments tailored to individual patient characteristics to mitigate risks.

## 6. New molecules identified via molecular docking could serve in developing more effective and safer drugs.

Molecular docking simulations identified compounds with high predicted binding affinities to receptors involved in cancer cell proliferation. These compounds represent potential candidates for further experimental validation and development of novel targeted oncological therapies with improved efficacy and reduced toxicity compared to conventional drugs.

#### 7. Treatment effects are dose- and time-dependent.

All analyzed studies demonstrated that therapeutic efficacy closely correlates with concentration and exposure duration. Tested substances exhibited stronger cytotoxic effects at higher doses and after longer incubation (48 hours versus 24 hours). This cumulative effect is critical for optimizing treatment regimens to avoid underdosing, which may lead to inefficacy, or overdosing, which may increase toxicity.

#### 8. Plant extracts and nanoparticles may help reduce chemotherapy side effects.

An important observation is that certain combinations of plant extracts and nanoparticles protected healthy cells from cytotoxic drug toxicity without compromising effects on cancer cells. This suggests that natural compound-based therapies could mitigate chemotherapy adverse effects, reduce patient discomfort and improve quality of life.

### 9. Pharmacological monitoring of oncological drugs must be enhanced to ensure patient safety.

Pharmacovigilance data highlight significant adverse drug reactions necessitating constant surveillance. Geographic variability in reporting points to a need for global standardization of side effect monitoring. Underreporting by patients may influence perceived drug safety, emphasizing the importance of improved patient education and stronger collaboration between patients and healthcare providers.

### 10. Personalized medicine could play a key role in optimizing oncological treatments.

Study results indicate that therapies do not affect all patients equally, and toxicity varies by age, sex, and other biological factors. Personalizing treatment based on each patient's genetic and metabolic profile could enhance therapeutic efficacy and reduce adverse effects. Implementing individualized treatment strategies may represent the future of oncology, offering better outcomes and greater treatment tolerability.

These general conclusions emphasize major research directions in oncology and antimicrobial treatment fields, highlighting advantages and challenges of nanoparticle use, plant extracts, and combined therapies. Future research should focus on experimental validation, formulation optimization, and integration of these strategies into clinical treatments to maximize patient benefits.

#### SELECTIVE BIBLIOGRAPHY

- 77. Becker, E.C., G. Ozcan, and G.Y. Wu, *Primary Hepatic Extra-gastrointestinal Stromal Tumors: Molecular Pathogenesis, Immunohistopathology, and Treatment.* Journal of Clinical and Translational Hepatology, 2023. **11**(4): p. 942.
- 223. Parsania, et al., Chelidonium majus L. alkaloid extract enhances TRAIL-induced apoptosis in HeLa cell line through death receptors 4 and 5 upregulation. Gene Reports, 2021. 25: p. 101311.
- 224. Shen, L., Lee, S., Joo, J. C., Hong, E., Cui, Z. Y., Jo, E., Jang, H. J. et. al, *Chelidonium majus induces apoptosis of human ovarian cancer cells via ATF3-mediated regulation of Foxo3a by Tip60.* Journal of microbiology and biotechnology, 2022. **32**(4): p. 493.
- 225. Ahmad, et al., Differential antiproliferative and apoptotic response of sanguinarine for cancer cells versus normal cells. Clinical cancer research, 2000. **6**(4): p. 1524–1528.
- 226. Ahsan, et al., Sanguinarine induces apoptosis of human pancreatic carcinoma AsPC-1 and BxPC-3 cells via modulations in Bcl-2 family proteins. Cancer letters, 2007. **249**(2): p. 198–208.
- 227. Vrba, et al., Chelerythrine and dihydrochelerythrine induce G1 phase arrest and bimodal cell death in human leukemia HL-60 cells. Toxicology in vitro, 2008. 22(4): p. 1008–1017.
- 228. Noureini, et al., *Transcriptional down regulation of hTERT and senescence induction in HepG2 cells by chelidonine.* World Journal of Gastroenterology, 2009. **15**(29): p. 3603.
- 229. Vrba, et al., *Cytotoxic activity of sanguinarine and dihydrosanguinarine in human promyelocytic leukemia HL-60 cells*. Toxicology in vitro, 2009. **23**(4): p. 580–588.
- 230. Qu, et al., Chelidonine induces mitotic slippage and apoptotic-like death in SGC-7901 human gastric carcinoma cells. Molecular Medicine Reports, 2016. **13**(2): p. 1336–1344.
- 231. Havelek, et al., Comparative cytotoxicity of chelidonine and homochelidonine, the dimethoxy analogues isolated from Chelidonium majus L.(Papaveraceae), against human leukemic and lung carcinoma cells. Phytomedicine, 2016. **23**(3): p. 253–266.
- 232. Jang, et al., Chelidonine induces apoptosis via GADD45a-p53 regulation in human pancreatic cancer cells. Integrative Cancer Therapies, 2021. **20**.
- 233. Lin, et al., Chelerythrine-induced apoptotic cell death in HepG2 cells involves the inhibition of Akt pathway and the activation of oxidative stress and mitochondrial apoptotic pathway. Antioxidants, 2022. 11(9): p. 1837.
- 234. Biswas, et al., *Efficacy of a plant extract (Chelidonium majus L.) in combating induced hepatocarcinogenesis in mice.* Food and Chemical Toxicology, 2008. **46**(5): p. 1474–1487.
- 235. Mikołajczak, et al., Evaluation of anti-inflammatory and analgesic activities of extracts from herb of Chelidonium majus L. Central European Journal of Immunology, 2015. **40**(4): p. 400–410.
- VI and S, *Analysis of total phenols and other oxidation substrates and antioxidants by means of Folin-Ciocalteu reagent.* Methods in Enzymology, 1999. **299**: p. 152–178.
- 237. Waisundara, V., Antioxidants: Benefits, Sources, Mechanisms of Action. 2021: IntechOpen.
- 238. Sarwar, et al., Evaluation of antioxidant, free radical scavenging, and antimicrobial activity of Quercus incana Roxb. Frontiers in Pharmacology, 2015. **6**: p. 277.
- Yue, et al., *Structural insight into apelin receptor-G protein stoichiometry*. Nature structural & molecular biology, 2022. **29**(7): p. 688–697.
- 248. Ring, et al., Adrenaline-activated structure of  $\beta$ 2-adrenoceptor stabilized by an engineered nanobody. Nature, 2013. **502**(7472): p. 575–579.
- 249. Cai, et al., *Structures of adenosine receptor A2BR bound to endogenous and synthetic agonists.* Cell Discovery, 2022. **8**(1): p. 140.
- 250. Laskowski, et al., *PDBsum: Structural summaries of PDB entries.* Protein science, 2018. **27**(1): p. 129–134.
- 252. O'Boyle, et al., *Open Babel: An open chemical toolbox*. Journal of cheminformatics, 2011. **3**: p. 1–14.

#### Annex 4 – Scientific Works

#### 4.1 Full-length papers published as first author in ISI-ranked journals indexed in Web of Science:

- **4.1.1** <u>Mirela Claudia Rimbu</u>, Liliana Popescu, Mirela Mihăilă, Roxana Colette Sandulovici, Daniel Cord, Carmen Marinela Mihailescu, Mona Luciana Galatanu, Mariana Panturoiu, Carmen Elisabeta Manea, Adina Boldeiu, Oana Brincoveanu, Mihaela Savin, Alexandru Grigoroiu, Florin Dan Ungureanu, Emilia Amzoiu, Mariana Popescu, Elena Truta, *Synergistic Effects of Green Nanoparticles on Antitumor Drug Efficacy in Hepatocellular Cancer*, Biomedicines 2025, 13, 641, <a href="https://doi.org/10.3390/biomedicines13030641">https://doi.org/10.3390/biomedicines13030641</a>, **FI=3,9**
- **4.1.2** <u>Mirela Claudia Rimbu</u>, Dan Florin Ungureanu, Cosmin Modovan, Madalina Toba, Marinela Chirila, Elena Truta, Daniel Cord, *Cystic Hepatic GIST: A Case Report of Rare Presentation and Long-Term Survival*, Curr. Oncol. 2025, 32, 383 https://doi.org/10.3390/curroncol32070383, FI=3,4
- **4.1.3** <u>Mirela Claudia Rimbu</u>, Daniel Cord, Mihaela Savin, Alexandru Grigoroiu, Mirela Antonela Mihăilă, Mona Luciana Gălățanu, Viorel Ordeanu, Mariana Panțuroiu, Vasilica Țucureanu, Iuliana Mihalache, Oana Brîncoveanu, Adina Boldeiu, Veronica Anăstăsoaie, Carmen Elisabeta Manea, Roxana Colette Sandulovici, Marinela Chirilă, Adina Turcu Știololică, Emilia Amzoiu, Victor Eduard Peteu, Cristiana Tănase, Bogdan Firtat, Crmen Marinela Mihăilescu, *Harnessing Plant-Based Nanoparticles for Targeted Therapy: A Green Approach to Cancer and Bacterial Infections, Int. J. Mol. Sci.* **2025**, *26*(14), 7022; https://doi.org/10.3390/ijms26147022 (registering DOI) <a href="https://www.mdpi.com/1422-0067/26/14/7022">https://www.mdpi.com/1422-0067/26/14/7022</a>, **FI:4,9**
- **4.1.4** Daniel Cord, Mirela Claudia Rimbu autor corespondent, Cristiana Tănase, Cristina Tăbleț, Gheorghe Duca, Molecular docking study of some active principles from Silybum marianum, Chelidonium majus, Ginkgo biloba, Gelsemim sempervirens, Artemisia annua and Taraxacum officinale, Chemistry Journal of Moldova. General, Industrial and Ecological Chemistry. 2025, 20(1), 100-105 https://doi.org/10.19261/cjm.2025.1337, FI=0,5

#### 4.2 Full-length papers published as first author (or co-author) in journals indexed in PubMed:

**4.2.1** Daniel Cord, <u>Mirela Claudia Rimbu</u> – autor corespondent, Liliana Popescu, *New prospects in oncotherapy: bioactive compounds from Taraxacum officinale*, Medicine and Pharmacy Reports, <a href="https://doi.org/10.15386/mpr-2875">https://doi.org/10.15386/mpr-2875</a>

#### 4.3 Papers presented as first author (or co-author) at national and international scientific events:

- **4.3.1** Daniel Cord, <u>Mirela Claudia Rimbu</u>, Cristiana Tanase, *Alkaloid Constituents of Chelidonium majus L.: An Overview of Their Biological Activity and Toxicity*, Conferința cu participare internațională a Facultății de Medicină a Universității Titu Maiorescu, Abordări inovatoare transdisciplinare în medicina modernă, ediția a VIII-a, București, 16-18 mai 2025
- **4.3.2** <u>Mirela Claudia Rîmbu</u>, Daniel Cord, Raluca Neacșa, Cristiana Tănase, Mariana Popescu, *Chemopreventive potential of Taraxacum officinale: a natural approach to cancer prevention* (Abstract), International Conference, Education and creativity for a knowledge based society (18th edition), Universitatea Titu Maiorescu, november 21 23, 2024, București
- **4.3.3** Mariana Panţuroiu, Mona Luciana Galăţanu, Luiza Mădălina Cima, Roxana Măriuca Gavriloaia, Roxana Colette Sandulovici, Mariana Popescu, Daniel Cord, <u>Mirela Claudia Rîmbu</u>, Evaluation of antioxidant activity and bioactive compound content in Silybum marianum, Cynara scolymus and Taraxacum officinale: Synergistic potential and therapeutic implications, International Conference, Education and creativity for a knowledge based society (18th edition), Universitatea Titu Maiorescu, november 21 23, 2024, Bucuresti
- **4.3.4** Mirela Mihăilă, Marinela Bostan, Viviana Roman, Camelia Hotnog, Mariana Popescu, Roxana Colette Sandulovici, Daniel Cord, <u>Mirela Claudia Rimbu</u>, *Compositional study and evaluation of the antiproliferative action of Chelidonium majus extract on tumor cell lines*, Al 10-lea Congres al Federației Societății Române de Cancer, al 30-lea Congres al Societății Române de Radioterapie și Oncologie Medicală, 24-27.10.2024, Sinaia, România (poster)
- **4.3.5** <u>Rîmbu Mirela</u>, Toba Mădălina Elena, Moldovan Cosmin, Ungureanu Florin Dan, *New developments in the correlation of imaging with the diagnosis and evolution of gastrointestinal stromal tumours*, Conferința cu participare internațională a Facultății de Medicină a Universității Titu Maiorescu, Abordări inovatoare transdisciplinare în medicina modernă, ediția a VI-a (01-03 iunie 2023)
- **4.3.6** Mariana Panțuroiu, Mona Luciana Gălățanu, <u>Mirela Claudia Rîmbu</u>, *The anticance effect of polyphenols*, International Conference, Education and creativity for a knowledge based society (16th edition), Universitatea Titu Maiorescu, november 24 26, 2022, București